



## Charge convection and interfacial deformation of a compound drop in plane Poiseuille flow under an electric field

Manash Protim Boruah,<sup>1</sup> Pitambar R. Randive,<sup>1</sup> Sukumar Pati ,<sup>1</sup> and Kirti Chandra Sahu <sup>2,\*</sup>

<sup>1</sup>*Department of Mechanical Engineering, National Institute of Technology Silchar, Silchar-788 010, India*

<sup>2</sup>*Department of Chemical Engineering, Indian Institute of Technology Hyderabad, Sangareddy, Telangana 502 284, India*



(Received 23 October 2021; accepted 6 January 2022; published 26 January 2022)

The electrohydrodynamics of a concentric compound drop migrating and deforming in a plane Poiseuille flow under the influence of an arbitrarily orientated uniform electric field is investigated using a double asymptotic approach with the electric Reynolds number and capillary number as small perturbation parameters. The effect of viscosity, conductivity, and permittivity ratios, the orientation of the applied electric field, and radius ratio is thoroughly investigated, and the underlying physics is examined in terms of surface charge distribution and shape deformation of the shell and core of the compound drop. For an undeformable compound drop, we found that as the radius ratio increases, the magnitude of lateral velocity due to charge convection increases for both the shell and core, while the longitudinal velocity decreases. The intensity of the drop to lag behind the imposed flow increases as the electric field strength increases. For deformable compound drops, it is observed that the influence of the tilt angle of the applied electric field in altering the direction of motion gets dampened out or minimized when the size of the core increases. We also find that under the combined action of charge convection and shape deformation, the increase in electric Reynolds number enhances the lateral velocity of both the shell and the core drop while the longitudinal velocity decreases. However, it is found that the magnitude of the lateral and longitudinal velocity of the shell and core drop increases with an increase in the capillary number. Finally, by solving for the velocity field of an eccentric compound drop under plane Poiseuille flow and subjected to an applied electric field, we show that there is a critical eccentricity limit and critical time limit within which the concentric and eccentric compound drop configurations produce similar results and beyond which the increment or decrement in shell and core drop velocity is dictated by the value of eccentricity.

DOI: [10.1103/PhysRevFluids.7.013703](https://doi.org/10.1103/PhysRevFluids.7.013703)

### I. INTRODUCTION

Ever since the pioneering work by Taylor [1], electric fields have been successfully employed to control the dynamics of weakly conducting dielectric liquid and attracted significant attention of researchers due to its appealing physics [2,3], as well as its relevance in a wide range of technological applications, such as microfluidics [4–6], biological systems [7], natural phenomena [8], atomization [9], to name a few. Several researchers [10–17] have investigated the deformation of neutrally buoyant droplets in an otherwise quiescent medium under uniform or nonuniform electric fields, considering leaky and conducting fluids, as well as in bounded and unbounded domains,

---

\*ksahu@che.iith.ac.in

using an approach similar to that of Taylor [1]. These studies were premised on the underlying physics that, in addition to normal stresses, electrical property contrast between the droplet and the surrounding medium causes the accumulation of free charges at the interface, resulting in tangential stresses, which generate circulatory toroidal currents (also known as Taylor vortices) inside the drop. The influence of interfacial velocity on the ensuing fluid flow due to a nonlinear coupling of charge distribution has been investigated using various computational fluid dynamics approaches (e.g., [18–21]). On the theoretical side, Bandopadhyay *et al.* [22] investigated the dynamics of a drop sedimenting under gravity while being subjected to an electric field, using double asymptotic expansions in the electric capillary number ( $Ca_E$ ) and electric Reynolds number ( $Re_E$ ), that balances the electric and viscous stresses. A similar problem was also studied by Yariv and Almog [23] for arbitrary electric Reynolds numbers.

A “compound drop” or “double emulsion” (a smaller core drop encapsulated by a larger shell drop, and the shell drop itself is suspended inside an immiscible medium) mimics several essential physical features involved with lipid bilayer formation [24], oil recovery through porous structures [25], phase separation [26], drug delivery [27], and raindrops [28,29]. Thus, many researchers have investigated the dynamics of compound drops without any external electric forcing in creeping flow [30,31], inertia [32], and under imposed uniaxial and biaxial extensional flows [25]. As the external electric field has been proved to be an effective tool in altering the transportation of single droplets, researchers have also recently examined the influence of external electric fields on the dynamics of compound droplets.

Gouz and Sadhal [33] was the first to report on the electrohydrodynamic stability of eccentric compound drops, translating under buoyancy in the creeping flow regime using a semianalytical approach in conjunction with a leaky dielectric model for spherical drops in bipolar coordinates, and concluded that stable equilibrium configurations are only attainable with the presence of an electric field. By conducting a combined numerical and experimental investigation, Tsukada *et al.* [34] showed that the degree of deformation and the flow strength correlated positively with both the electric field strength and the volume ratio of the core phase to the shell phase of a compound droplet. In the framework of leaky-dielectric theory and in the limit of small electric field strength and fluid inertia, Behjatian and Esmaeeli [35] analytically studied the behavior of compound drop and observed four possible flow patterns in and around the globule, in terms of the direction of the external flow and the number of vortices (single vortex and double vortices) in the shell. Soni *et al.* [36] used the phase-field method to understand the deformation dynamics of double emulsion droplet in a uniform electric field and observed prolate-oblate, prolate-prolate and oblate-prolate deformation. Subsequently, they also investigated the effect of alternating current (AC) electric field on the dynamics of a compound drop [37,38]. Borthakur *et al.* [39] numerically investigated the dynamics of deformation and pinch-off of a migrating compound droplet in a tube. Furthermore, Borthakur *et al.* [40] showed that the ratio of electrical permittivity and conductivity between the two phases plays a critical role in deciding the magnitude of deformation and orientation of the compound droplet subjected to the combined influence of electric field and shear flow.

Recently, Santra *et al.* [41,42] studied the pinch-off dynamics of a compound droplet subjected to a transverse electric field in Poiseuille and confined shear flows, respectively. They found a deviation of the inner droplet from the concentric position that finally leads to the pinch-off of the outer shell. In another study, Santra *et al.* [43] examined the combined influence of electrohydrodynamics and channel confinement on the transient behavior of a compound droplet. Under the assumption of negligible fluid inertia and small shape deformation, the authors have also developed an asymptotic model to predict the transient as well as the steady-state behavior of the compound droplet for the limiting case of an unbounded suspending medium. However, none of the aforementioned literature on compound drop considered the effect of surface charge convection in dictating the involved electrohydrodynamics facets. Moreover, the electric and hydrodynamic stresses can lead to shape deformation which can reversely alter the electrohydrodynamics characteristics of compound drops. These two key determinants viz. shape deformation and charge convection have played a pivotal role

in the rotation rate, effective shear viscosity, and normal stress difference of simple drops as reported in previous studies [11,22].

The above discussion clarifies that it remains open for the researchers to bring out the confluence of an electric field and an externally imposed background flow field in dictating the motion and deformation of compound drop under the combined consideration of surface charge convection and shape deformation, which is the main objective of the current study. Moreover, unlike prior works [41,42] that only evaluated the effect of the capillary number (Ca) as a single perturbation parameter, we adopt a twofold asymptotic approach with the electric Reynolds number ( $Re_E$ ) and the capillary number (Ca) as small perturbation parameters, and develop a three-dimensional formalism for a compound drop migrating in a Poiseuille flow under the influence of an applied electric field. Under the framework of negligible fluid inertia and small shape deformation, our study captures the influence of an applied electric field direction, hydrodynamic and electric properties, and compound droplet size in dictating the migration velocity of compound drop. Unlike the case of a single drop, our study reveals that the radius ratio of the compound drop acts as a novel trigger in controlling the deformation and migration of the drop under the confluence of other electrohydrodynamic parameters.

The rest of the paper is organized as follows. The problem is formulated in Sec. II. The results from the numerical simulations are discussed in Sec. III. Finally, conclusions are given in Sec. IV.

## II. FORMULATION

### A. Physical configuration

We investigate the electrohydrodynamics of a concentric leaky dielectric compound drop of undeformed outer radius  $R_o$  and undeformed inner radius  $R_i$  in a plane Poiseuille flow configuration under a uniform electric field [ $\mathbf{E}_\infty = E_c(E_x \mathbf{e}_x + E_z \mathbf{e}_z)$ ] applied in an arbitrary orientation quantified by a tilt angle,  $\theta_t = \tan^{-1}(E_x/E_z)$  and  $E_x^2 + E_z^2 = 1$ . Here,  $E_c$  is the characteristic electric field;  $E_x$ ,  $\mathbf{e}_x$  and  $E_z$ ,  $\mathbf{e}_z$  are the components of the electric field and the corresponding unit vectors in the  $x$  and  $z$  directions, respectively. It is assumed that the droplet is far away from the walls. A schematic diagram (not to scale) is shown in Fig. 1(a). The rigid and impermeable walls of infinite width along the  $y$  and  $z$  directions are separated by a distance  $H$  in the  $x$  direction. Thus, the imposed plane Poiseuille flow in a Cartesian coordinate system considering the drop centroid as origin can be expressed as

$$\mathbf{V}_\infty = V_c(k_0 + k_1x + k_2x^2)\mathbf{e}_z, \quad (1)$$

where,  $V_c$  is the characteristic velocity;  $k_0 = 4(x_d/H)(1 - x_d/H)$ ,  $k_1 = 4(1 - 2x_d/H)/H$  and  $k_2 = -4/H^2$ . The outer and inner drop are assumed to move at velocities  $\mathbf{U}_2$  and  $\mathbf{U}_3$ , respectively.

A spherical coordinate system  $(r, \theta, \phi)$  with its origin attached to the centroid of the compound drop is employed. The fluids are assumed to be incompressible, Newtonian and immiscible. The outermost phase (the suspending medium), the outer (shell region) and the inner (core region) phases of the compound droplet are represented by fluid 1, fluid 2, and fluid 3, respectively, and we use these numbers to denote the corresponding fluid and electrical properties, such as density ( $\rho_i$ ), viscosity ( $\mu_i$ ), electrical permittivity ( $\varepsilon_i$ ), and electrical conductivity ( $\sigma_i$ ), where  $i = 1, 2$ , and 3. We also use subscript  $ij$  to represent the interface separating the  $i$ th and  $j$ th fluids. Thus,  $\gamma_{ij}$  represents the surface tension at the interface separating the  $i$ th and  $j$ th fluids.

### B. Nondimensionalization

We nondimensionalize the length by  $R_o$ ; velocity by  $V_c$ ; electric field by  $E_c$ ; hydrodynamic stress by  $\tau_{\text{ref}}^H (\equiv \mu_1 V_c / R_o)$ ; and electric stress by  $\tau_{\text{ref}}^E (\equiv \varepsilon E_c^2)$ . Similarly, the properties are scaled by the corresponding properties of the suspending medium resulting in three different ratios, namely, the viscosity ratio ( $\lambda_{1i} = \mu_i / \mu_1$ ), conductivity ratio ( $R_{1i} = \sigma_i / \sigma_1$ ), permittivity ratio ( $S_{1i} = \varepsilon_i / \varepsilon_1$ ), and radius ratio ( $K = R_i / R_o$ ). The choice of the aforementioned nondimensional scheme results in three

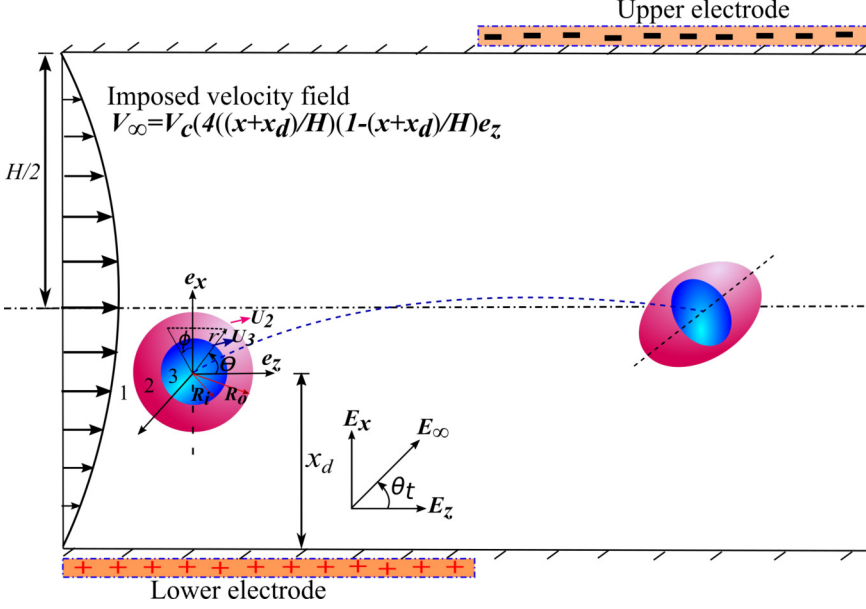


FIG. 1. (a) Schematic (not to scale) of a concentric compound drop with inner radius  $R_i$  and outer radius  $R_o$  in a plane Poiseuille flow field ( $\mathbf{V}_\infty$ ) and under a uniform electric field  $\mathbf{E}_\infty$  oriented at an angle  $\theta_t$  (termed as tilt angle) with respect to the axial direction. Initially, the compound drop is placed at a transverse position  $x_d$  (measured from the bottom wall).

important dimensionless numbers, viz. the Capillary number ( $\text{Ca} = \mu_1 V_c / \gamma_{12}$ ) which signifies the relative magnitude of the viscous force relative to the surface tension force, the Mason number ( $M = R_o \varepsilon_1 E_c^2 / \mu_1 V_c$ ) which signifies the ratio of the electrical stress to the viscous stress and the electric Reynolds number ( $\text{Re}_E = \varepsilon_1 V_c / R_o \sigma_1$ ) which is the ratio of the charge relaxation timescale ( $\varepsilon_1 / \sigma_1$ ) to the convective timescale ( $R_o / V_c$ ). The hydrodynamic Reynolds number for each phase, as well as the hydrodynamic capillary number are assumed to be small enough that the Stokes equations hold and the drops remain spherical. The justifications to the assumptions considered in this study are provided in Appendix A. In the next section, we will present the governing equations and boundary conditions for the electrostatic and hydrostatic problem in the dimensionless form and maintain the same dimensionless notation thereafter unless otherwise specified.

### C. Governing equations and boundary conditions

#### 1. Electrostatic

According to the leaky dielectric theory of Taylor [1], the electric potential ( $\psi_i$ ) for the  $i$ th fluid can be expressed as

$$\nabla^2 \psi_i = 0, \quad (2)$$

which is solved using the following boundary conditions [44,45]. (i) The electric potential at a distance far away from the droplet approaches the externally imposed electric potential (i.e., as  $\mathbf{r} \rightarrow \infty$ ,  $\psi_i \rightarrow -\mathbf{E}_\infty \cdot \mathbf{r}$ ). (ii) The electric potential is finite and bounded inside the core drop. (iii) The continuity of the electric potential is maintained at the two deformed interfaces (i.e., at  $\mathbf{r} = \mathbf{r}_{\Pi_{ij}}$ ,  $[\psi_i]_{\Pi_{ij}} = [\psi_j]_{\Pi_{ij}}$ ). Here,  $\mathbf{r}_{\Pi_{ij}} = 1 + f_{ij}(\theta, \phi)$  denotes the radial position of the deformed interfaces, where  $f_{ij}(\theta, \phi)$  represents the deviation of the  $ij$ th interface from sphericity,  $\Pi_{ij}$  refers to the interface of the  $i$ th and  $j$ th fluids and  $[\ ]_{\Pi_{ij}}$  symbolizes the evaluation of the bracketed quantity at the interface  $ij$ . (iv) The interfacial charge conservation at the steady state is satisfied by the electric



potential at the deformed  $ij$ th interface. Mathematically, it is given by

$$\mathbf{n}_{ij} \cdot (R_{1j} \nabla \psi_j - R_{1i} \nabla \psi_i) = -\text{Re}_E \nabla_s \cdot (q_{s,ij} \mathbf{V}_{s,ij}) \quad \text{at } \mathbf{r} = \mathbf{r}_{\Pi ij}, \quad (3)$$

where  $R_{1i} = \delta_{i1} + R_{12} \delta_{i2} + R_{13} \delta_{i3}$ . Here,  $\mathbf{n}_{ij} = \nabla(\mathbf{r} - \mathbf{r}_{\Pi ij}) / |\nabla(\mathbf{r} - \mathbf{r}_{\Pi ij})|$  denotes the outward normal unit vector at the deformed interfaces of the droplet,  $\nabla_s = \nabla_{ij} - \mathbf{n}_{ij}(\mathbf{n}_{ij} \cdot \nabla_{ij})$  is the surface gradient operator,  $q_{s,ij} = (S_{1j} \nabla \psi_j - S_{1i} \nabla \psi_i) \cdot \mathbf{n}_{ij}$  denotes the surface charge density, wherein  $S_{1i} = \delta_{i1} + S_{12} \delta_{i2} + S_{13} \delta_{i3}$ , and  $\mathbf{V}_{s,ij}$  is the surface velocity.

## 2. Hydrodynamic

Under the creeping flow condition, the velocity and pressure fields are governed by the following continuity and Stokes equation [46]

$$\nabla \cdot \mathbf{u}_i = 0, \quad \nabla p_i = \lambda_{1i} \nabla^2 \mathbf{u}_i, \quad (4)$$

where  $\mathbf{u}_i$  and  $p_i$  represent the velocity and pressure fields of phase  $i$ , respectively, and  $\lambda_{1i} = \delta_{i1} + \lambda_{12} \delta_{i2} + \lambda_{13} \delta_{i3}$ . The hydrodynamic equations are solved using the following boundary conditions. (i) The velocity field is uniform at a distance far away from the compound droplet, i.e., at  $\mathbf{r} \rightarrow \infty$ ,  $\mathbf{u}_i = -\mathbf{U}_2$ . (ii) The velocity and pressure fields must be bounded inside the core drop. (iii) The velocity is continuous across the interfaces of the compound droplet, i.e., at  $\mathbf{r} = \mathbf{r}_{\Pi ij}$ ,  $[\mathbf{u}_i]_{\Pi ij} = [\mathbf{u}_j]_{\Pi ij}$ , and  $[\mathbf{u}_i \cdot \mathbf{n}_{ij}]_{\Pi ij} = [\mathbf{u}_j \cdot \mathbf{n}_{ij}]_{\Pi ij} = (\mathbf{U}_3 - \mathbf{U}_2) \cdot \mathbf{n}_{23} \delta_{i2} \delta_{j3}$ . (iv) At steady state, the force acting at the interface due to the jump in hydrodynamic and electric stresses is balanced by the capillary stress, which is mathematically given by

$$[\mathbf{n}_{ij} \cdot (\boldsymbol{\tau}_j^H + M \boldsymbol{\tau}_j^E) \cdot \mathbf{n}_{ij}]_{\Pi ij} - [\mathbf{n}_{ij} \cdot (\boldsymbol{\tau}_i^H + M \boldsymbol{\tau}_i^E) \cdot \mathbf{n}_{ij}]_{\Pi ij} = \frac{1}{\text{Ca}} (\nabla \cdot \mathbf{n}_{ij}), \quad (5)$$

where  $\boldsymbol{\tau}_i^H = -p_i \mathbf{I} + \lambda_{1i} [\nabla \mathbf{u}_i + (\nabla \mathbf{u}_i)^T]$  and  $\boldsymbol{\tau}_i^E = S_i [E_i E_i^T - |E_i|^2 \mathbf{I}/2]$  are the viscous and electric stress tensors, respectively.

## D. Asymptotic perturbation analysis

As in many microfluidics applications,  $\text{Re}_E \ll 1$ ,  $\text{Ca} \gg \text{Re}_E^2$ ,  $\text{CaRe}_E$ ,  $\text{Ca}^2$ , it allows us to consider  $\text{Ca}$  and  $\text{Re}_E$  as perturbation parameters [11,45]. Thus, a double asymptotic expansion of any pertinent variable,  $\Gamma$  can be expanded as

$$\Gamma = \Gamma^{(0)} + \text{Ca} \Gamma^{(\text{Ca})} + \text{Re}_E \Gamma^{(\text{Re}_E)} + O(\text{Re}_E^2, \text{CaRe}_E, \text{Ca}^2), \quad (6)$$

that can aid in linearizing the problem. Here,  $\Gamma^{(0)}$  is the leading-order term associated with the ascent of the interfacial charge convection and shape deformation,  $\Gamma^{(\text{Re}_E)}$  denotes the first order correction due to the charge convection and  $\Gamma^{(\text{Ca})}$  indicates the first order correction due to the shape deformation. However, the regular perturbation equations for pressure and stress need to be modified as

$$p_i = \frac{1}{\text{Ca}} p_i^{(1/\text{Ca})} + p_i^{(0)} + \text{Ca} p_i^{(\text{Ca})} + \text{Re}_E p_i^{(\text{Re}_E)} + \dots, \quad (7)$$

$$\boldsymbol{\tau}_i = \frac{1}{\text{Ca}} \boldsymbol{\tau}_i^{(1/\text{Ca})} + \boldsymbol{\tau}_i^{(0)} + \text{Ca} \boldsymbol{\tau}_i^{(\text{Ca})} + \text{Re}_E \boldsymbol{\tau}_i^{(\text{Re}_E)} + \dots, \quad (8)$$

respectively. Here, we include the terms  $\frac{1}{\text{Ca}} p_i^{(1/\text{Ca})}$  and  $\frac{1}{\text{Ca}} \boldsymbol{\tau}_i^{(1/\text{Ca})}$  to balance the Laplace pressure across the interfaces of the compound drop [47].

The perturbation equation for the unknown shape of the deformed compound drop takes the following form:

$$r_{\Pi ij} = 1 + f_{ij}(\theta, \phi) = K_i (1 + \text{Ca} f_{ij}^{(\text{Ca})} + \text{CaRe}_E f_{ij}^{(\text{CaRe}_E)} + \text{Ca}^2 f_{ij}^{(\text{Ca}^2)}) + \dots, \quad (9)$$

with  $K_i = \delta_{i1} + K\delta_{i2}$ . Here  $f_{ij}^{(Ca)}$ ,  $f_{ij}^{(CaRe_E)}$  and  $f_{ij}^{(Ca^2)}$  are the corrections to the deformed shape of the compound drop at different orders of approximation. In perturbed form, the outward unit normal,  $\mathbf{n}_{ij}$  and the curvature of the deformed  $ij$ th interface,  $\nabla \cdot \mathbf{n}_{ij}$  can be expressed as [48–50]

$$\begin{aligned} \mathbf{n}_{ij} = \frac{\nabla(\mathbf{r} - \mathbf{r}_{\Pi ij})}{|\nabla(\mathbf{r} - \mathbf{r}_{\Pi ij})|} = & \mathbf{e}_r - Ca \nabla f_{ij}^{(Ca)} - CaRe_E \nabla f_{ij}^{(CaRe_E)} \\ & - Ca^2 \left[ \nabla f_{ij}^{(Ca^2)} + \frac{1}{2} (\nabla f_{ij}^{(Ca)} \cdot \nabla f_{ij}^{(Ca)}) \mathbf{e}_r \right], \end{aligned} \quad (10)$$

and

$$\begin{aligned} \nabla \cdot \mathbf{n}_{ij} = & 2 - Ca(2f^{(Ca)} + \nabla^2 f^{(Ca)}) - CaRe_E(2f^{(CaRe_E)} + \nabla^2 f^{(CaRe_E)}) \\ & - Ca^2 \{-2f^{(Ca)}(f^{(Ca)} + \nabla^2 f^{(Ca)}) + 2f^{(Ca^2)} + \nabla^2 f^{(Ca^2)}\} - \dots \end{aligned} \quad (11)$$

Using the aforementioned perturbation scheme, the governing equations and boundary conditions for the electrostatic (Sec. II C 1) and hydrodynamic (Sec. II C 2) problem transform into the following forms at leading order,  $O(Re_E)$  and  $O(Ca)$ .

### 1. Leading order

The governing equation for an electric field at leading order becomes

$$\nabla^2 \psi_i^{(0)} = 0, \quad (12)$$

and it is subjected to the following boundary conditions:

$$\psi_1^{(0)}|_{r \rightarrow \infty} \rightarrow -\mathbf{E}_\infty \cdot \mathbf{r}, \quad (13)$$

$$\psi_i^{(0)}|_{r=K_i} = \psi_j^{(0)}|_{r=K_i}, \quad (14)$$

$$\mathbf{e}_r \cdot (R_{1j} \nabla \psi_j^{(0)} - R_{1i} \nabla \psi_i^{(0)})|_{r=K_i} = 0. \quad (15)$$

The flow field satisfies the following governing equations at leading order

$$\nabla \cdot \mathbf{u}_i^{(0)} = 0, \quad \nabla p_i^{(0)} = \lambda_{1i} \nabla^2 \mathbf{u}_i^{(0)}, \quad (16)$$

and they are subjected to the following boundary conditions:

$$\mathbf{u}_1^{(0)}|_{r \rightarrow \infty} \rightarrow \mathbf{V}_\infty^{(0)} - \mathbf{U}_2^{(0)}, \quad (17)$$

$$\mathbf{u}_i^{(0)}|_{r=K_i} = \mathbf{u}_j^{(0)}|_{r=K_i}, \quad (18)$$

$$\mathbf{u}_i^{(0)}|_{r=K_i} \cdot \mathbf{e}_r = \mathbf{u}_j^{(0)}|_{r=K_i} \cdot \mathbf{e}_r = \delta_{i2} [(\mathbf{U}_3^{(0)} - \mathbf{U}_2^{(0)}) \cdot \mathbf{e}_r], \quad (19)$$

$$\mathbf{e}_r \cdot (\boldsymbol{\tau}_i^{(0)} - \boldsymbol{\tau}_j^{(0)})|_{r=K_i} \cdot (\mathbf{I} - \mathbf{e}_r \mathbf{e}_r) = 0, \quad (20)$$

$$\mathbf{e}_r \cdot (\boldsymbol{\tau}_i^{(0)} - \boldsymbol{\tau}_j^{(0)})|_{r=K_i} \cdot \mathbf{e}_r = -(2f^{(Ca)} + \nabla^2 f^{(Ca)}). \quad (21)$$

### 2. $O(Re_E)$ : Effect of surface charge convection

The governing equation for an electric field at  $O(Re_E)$  takes the following form:

$$\nabla^2 \psi_i^{(Re_E)} = 0, \quad (22)$$

and it is subjected to the following boundary conditions:

$$\psi_1^{(Re_E)}|_{r \rightarrow \infty} \rightarrow 0, \quad (23)$$

$$\psi_i^{(\text{Re}_E)}|_{r=K_i} = \psi_j^{(\text{Re}_E)}|_{r=K_i}, \quad (24)$$

$$\mathbf{e}_r \cdot (R_{1j} \nabla \psi_j^{(\text{Re}_E)} - R_{1i} \nabla \psi_i^{(\text{Re}_E)})|_{r=K_i} = -\nabla_s \cdot (q_{s,ij}^{(0)} \mathbf{V}_{s,ij}^{(0)})|_{r=K_i}. \quad (25)$$

The flow field satisfies the following governing equations at  $O(\text{Re}_E)$

$$\nabla \cdot \mathbf{u}_i^{(\text{Re}_E)} = 0, \quad \nabla p_i^{(\text{Re}_E)} = \lambda_{1i} \nabla^2 \mathbf{u}_i^{(\text{Re}_E)}, \quad (26)$$

and they are subjected to the following boundary conditions:

$$\mathbf{u}_1^{(\text{Re}_E)}|_{r \rightarrow \infty} \rightarrow -\mathbf{U}_2^{(\text{Re}_E)}, \quad (27)$$

$$\mathbf{u}_i^{(\text{Re}_E)}|_{r=K_i} = \mathbf{u}_j^{(\text{Re}_E)}|_{r=K_i}, \quad (28)$$

$$\mathbf{u}_i^{(\text{Re}_E)}|_{r=K_i} \cdot \mathbf{e}_r = \mathbf{u}_j^{(\text{Re}_E)}|_{r=K_i} \cdot \mathbf{e}_r = \delta_{i2} [(\mathbf{U}_3^{(\text{Re}_E)} - \mathbf{U}_2^{(\text{Re}_E)}) \cdot \mathbf{e}_r], \quad (29)$$

$$\mathbf{e}_r \cdot (\boldsymbol{\tau}_i^{(\text{Re}_E)} - \boldsymbol{\tau}_j^{(\text{Re}_E)})|_{r=K_i} \cdot (\mathbf{I} - \mathbf{e}_r \mathbf{e}_r) = 0, \quad (30)$$

$$\mathbf{e}_r \cdot (\boldsymbol{\tau}_i^{(\text{Re}_E)} - \boldsymbol{\tau}_j^{(\text{Re}_E)})|_{r=K_i} \cdot \mathbf{e}_r = -(2f^{(\text{CaRe}_E)} + \nabla^2 f^{(\text{CaRe}_E)}). \quad (31)$$

### 3. $O(\text{Ca})$ : Effect of concentric compound drop deformation

The governing equation for an electric field at  $O(\text{Ca})$  takes the following form:

$$\nabla^2 \psi_i^{(\text{Ca})} = 0, \quad (32)$$

and it is subjected to the following boundary conditions:

$$\psi_1^{(\text{Ca})}|_{r \rightarrow \infty} \rightarrow 0, \quad (33)$$

$$\psi_i^{(\text{Ca})}|_{r=K_i + \text{Ca}f_{ij}^{(\text{Ca})}} = \psi_j^{(\text{Ca})}|_{r=K_i + \text{Ca}f_{ij}^{(\text{Ca})}}, \quad (34)$$

$$\mathbf{n}_{ij} \cdot (R_{1j} \nabla \psi_j^{(\text{Ca})} - R_{1i} \nabla \psi_i^{(\text{Ca})})|_{r=K_i + \text{Ca}f_{ij}^{(\text{Ca})}} = 0. \quad (35)$$

The flow field satisfies the following governing equations at  $O(\text{Ca})$

$$\nabla \cdot \mathbf{u}_i^{(\text{Ca})} = 0, \quad \nabla p_i^{(\text{Ca})} = \lambda_{1i} \nabla^2 \mathbf{u}_i^{(\text{Ca})}, \quad (36)$$

and they are subjected to the following boundary conditions:

$$\mathbf{u}_1^{(\text{Ca})}|_{r \rightarrow \infty} \rightarrow -\mathbf{U}_2^{(\text{Ca})}, \quad (37)$$

$$\mathbf{u}_i^{(\text{Ca})}|_{r=K_i + \text{Ca}f_{ij}^{(\text{Ca})}} = \mathbf{u}_j^{(\text{Ca})}|_{r=K_i + \text{Ca}f_{ij}^{(\text{Ca})}}, \quad (38)$$

$$\mathbf{u}_i^{(\text{Ca})}|_{r=K_i + \text{Ca}f_{ij}^{(\text{Ca})}} \cdot \mathbf{n}_{ij} = \mathbf{u}_j^{(\text{Ca})}|_{r=K_i + \text{Ca}f_{ij}^{(\text{Ca})}} \cdot \mathbf{n}_{ij} = \delta_{i2} [(\mathbf{U}_3^{(\text{Ca})} - \mathbf{U}_2^{(\text{Ca})}) \cdot \mathbf{n}_{ij}], \quad (39)$$

$$\mathbf{n}_{ij} \cdot (\boldsymbol{\tau}_i^{(\text{Ca})} - \boldsymbol{\tau}_j^{(\text{Ca})})|_{r=K_i + \text{Ca}f_{ij}^{(\text{Ca})}} \cdot (\mathbf{I} - \mathbf{n}_{ij} \mathbf{n}_{ij}) = 0, \quad (40)$$

$$\mathbf{n}_{ij} \cdot (\boldsymbol{\tau}_i^{(\text{Ca})} - \boldsymbol{\tau}_j^{(\text{Ca})})|_{r=K_i + \text{Ca}f_{ij}^{(\text{Ca})}} \cdot \mathbf{n}_{ij} = 2f_{ij}^{(\text{Ca})} (f_{ij}^{(\text{Ca})} + \nabla^2 f_{ij}^{(\text{Ca})}) - (2f_{ij}^{(\text{Ca}^2)} + \nabla^2 f_{ij}^{(\text{Ca}^2)}). \quad (41)$$

Note that the generic term of the form  $\Gamma_i^{(\text{Ca})}|_{r=K_i + \text{Ca}f_{ij}^{(\text{Ca})}}$  used above represents the  $O(\text{Ca})$  evaluation of that generic quantity  $\Gamma$  of the  $i$ th phase at the deformed  $ij$ th interface ( $\mathbf{r} = K_i + \text{Ca}f_{ij}^{(\text{Ca})}$ ) of the compound drop. The terms of this form can be expanded using the Taylor series about  $\mathbf{r} = K_i$

and by collecting the  $O(\text{Ca})$  terms, we get

$$\Gamma_i^{(\text{Ca})}\Big|_{r=K_i+\text{Ca}f_{ij}^{(\text{Ca})}} = \Gamma_i^{(\text{Ca})}\Big|_{r=K_i} + f_{ij}^{(\text{Ca})} \frac{\partial \Gamma_i^{(\text{Ca})}}{\partial r}\Big|_{r=K_i}. \quad (42)$$

#### 4. Description of field variables

The solution of the governing Laplace equation for electric potential in the suspending medium ( $i = 1$ ), shell region ( $i = 2$ ) and core region ( $i = 3$ ) of the compound drop can be expressed in terms of solid spherical harmonics as

$$\psi_1^{(k)} = -E_\infty \cdot \mathbf{r} + \sum_{n=0}^{\infty} r^{-n-1} \sum_{m=0}^n [a_{-n-1,m}^{(k)} \cos(m\phi) + \hat{a}_{-n-1,m}^{(k)} \sin(m\phi)] P_{n,m}(\cos\theta), \quad (43)$$

$$\begin{aligned} \psi_2^{(k)} &= \sum_{n=0}^{\infty} r^n \sum_{m=0}^n [b_{n,m}^{(k)} \cos(m\phi) + \hat{b}_{n,m}^{(k)} \sin(m\phi)] P_{n,m}(\cos\theta) \\ &+ \sum_{n=0}^{\infty} r^{-n-1} \sum_{m=0}^n [b_{-n-1,m}^{(k)} \cos(m\phi) + \hat{b}_{-n-1,m}^{(k)} \sin(m\phi)] P_{n,m}(\cos\theta), \end{aligned} \quad (44)$$

$$\psi_3^{(k)} = \sum_{n=0}^{\infty} r^n \sum_{m=0}^n [c_{n,m}^{(k)} \cos(m\phi) + \hat{c}_{n,m}^{(k)} \sin(m\phi)] P_{n,m}(\cos\theta), \quad (45)$$

where  $k$  indicates the order of perturbations viz. 0,  $\text{Re}_E$  and  $\text{Ca}$ .  $P_{n,m}(\cos\theta)$  represents the associated Legendre polynomial of degree  $n$  and order  $m$  with argument  $\cos\theta$ . The hydrodynamic problem is solved using the Lamb's general solution procedure [51] for Stokes equation, according to which the velocity and the pressure fields at different order of perturbations ( $k = 0, \text{Re}_E,$  and  $\text{Ca}$ ) can be expressed in the following form:

$$\begin{aligned} \mathbf{u}_1^{(k)} &= \mathbf{V}_\infty^{(k)} - \mathbf{U}_2^{(k)} + \sum_{n=1}^{\infty} \left[ \nabla \times (\mathbf{r} \chi_{-n-1}^{(k)(1)}) \right. \\ &\quad \left. + \nabla \phi_{-n-1}^{(k)(1)} - \frac{n-2}{2n(2n-1)} r^2 \nabla p_{-n-1}^{(k)(1)} + \frac{n+1}{n(2n-1)} \mathbf{r} p_{-n-1}^{(k)(1)} \right], \end{aligned} \quad (46)$$

$$p_1^{(k)} = \sum_{n=1}^{\infty} p_{-n-1}^{(k)(1)}, \quad (47)$$

$$\begin{aligned} \mathbf{u}_2^{(k)} &= \sum_{n=1}^{\infty} \left[ \nabla \times \{ \mathbf{r} (\chi_n^{(k)(2)} + \chi_{-n-1}^{(k)(2)}) \} + \nabla (\phi_n^{(k)(2)} + \phi_{-n-1}^{(k)(2)}) \right. \\ &\quad \left. + \left\{ \frac{n+3}{2(n+1)(2n+3)\lambda_2} r^2 \nabla p_n^{(k)(2)} - \frac{n-2}{2n(2n-1)\lambda_2} r^2 \nabla p_{-n-1}^{(k)(2)} \right\} \right. \\ &\quad \left. - \left\{ \frac{n}{(n+1)(2n+3)\lambda_2} \mathbf{r} p_n^{(k)(2)} - \frac{n+1}{n(2n-1)\lambda_2} \mathbf{r} p_{-n-1}^{(k)(2)} \right\} \right], \end{aligned} \quad (48)$$

$$p_2^{(k)} = \sum_{n=1}^{\infty} (p_n^{(k)(2)} + p_{-n-1}^{(k)(2)}), \quad (49)$$

$$\begin{aligned} \mathbf{u}_3^{(k)} &= \sum_{n=1}^{\infty} \left[ \nabla \times (\mathbf{r} \chi_n^{(k)(3)}) + \nabla \phi_n^{(k)(3)} + \frac{n+3}{2(n+1)(2n+3)\lambda_3} r^2 \nabla p_n^{(k)(3)} \right. \\ &\quad \left. - \frac{n}{(n+1)(2n+3)\lambda_3} \mathbf{r} p_n^{(k)(3)} \right], \end{aligned} \quad (50)$$

$$p_3^{(k)} = \sum_{n=1}^{\infty} p_n^{(k)(3)}. \quad (51)$$

Here  $p_n^{(k)(i)}$ ,  $\phi_n^{(k)(i)}$ , and  $\chi_n^{(k)(i)}$  represent the growing solid harmonics and  $p_{-n-1}^{(k)(i)}$ ,  $\phi_{-n-1}^{(k)(i)}$ , and  $\chi_{-n-1}^{(k)(i)}$  are the decaying solid harmonics, the expressions of which are provided in Appendix B.

Moreover, the corrections to the deformed shape of the compound drop ( $f_{ij}^{(\text{Ca})}$ ,  $f_{ij}^{(\text{CaReE})}$  and  $f_{ij}^{(\text{Ca}^2)}$ ) can be expressed in spherical harmonic notations as

$$f_{ij}^{(\text{Ca})} = \sum_{n=1}^{\infty} [L_{n,m}^{(\text{Ca})(ij)} \cos(m\phi) + \hat{L}_{n,m}^{(\text{Ca})(ij)} \sin(m\phi)] P_{n,m}(\cos\theta), \quad (52)$$

where  $L_{n,m}^{(\text{Ca})(ij)}$  and  $\hat{L}_{n,m}^{(\text{Ca})(ij)}$  are the unknown coefficients.

### 5. Leading-order solution

At the leading order, we first employ the boundary conditions Eqs. (13)–(15) into (43)–(45) to determine the coefficients  $a_{-n-1,m}^{(0)}$ ,  $\hat{a}_{-n-1,m}^{(0)}$ ,  $b_{n,m}^{(0)}$ ,  $\hat{b}_{n,m}^{(0)}$ ,  $b_{-n-1,m}^{(0)}$ ,  $\hat{b}_{-n-1,m}^{(0)}$ ,  $c_{n,m}^{(0)}$ , and  $\hat{c}_{n,m}^{(0)}$ . Since the electric field is decoupled from the velocity field in this case, it finally results in the following expression for leading-order electric potential in the suspending medium, shell region and core region of the compound drop.

$$\begin{aligned} \psi_1^{(0)} &= \left(-r + \frac{\Omega\Lambda}{r^2}\right)(E_x \sin\theta \cos\phi + E_z \cos\theta), \\ \psi_2^{(0)} &= 3\Lambda \left(r + \frac{\xi}{r^2}\right)(2R_{12} + R_{13})(E_x \sin\theta \cos\phi + E_z \cos\theta), \\ \psi_3^{(0)} &= 9r\Lambda R_{12}(E_x \sin\theta \cos\phi + E_z \cos\theta), \end{aligned} \quad (53)$$

where  $\Omega$ ,  $\Lambda$ , and  $\xi$  are functions of  $K$ ,  $R_{12}$ , and  $R_{13}$  having the following form:

$$\Omega = K^3(2R_{12}^2 - 2R_{12}R_{13} + R_{12} - R_{13}) - (2R_{12}^2 + R_{12}R_{13} - 2R_{12} - R_{13}), \quad (54)$$

$$\Lambda = 1/[2K^3(R_{12}^2 - R_{12}R_{13} - R_{12} + R_{13}) - (2R_{12}^2 + R_{12}R_{13} + 4R_{12} + 2R_{13})], \quad (55)$$

$$\xi = K^3(R_{12} - R_{13})/(2R_{12} + R_{13}). \quad (56)$$

Using the solution for electric potentials, we can apply the relation,  $q_{s,ij} = (S_{1j}\nabla\psi_j - S_{1i}\nabla\psi_i) \cdot \mathbf{e}_r$  to determine the surface charge density at the two interfaces 12 and 23 as

$$q_{s,12}^{(0)} = -12(E_x \sin\theta \cos\phi + E_z \cos\theta) \left[ -\frac{1}{12} + \left\{ \left( \xi - \frac{1}{2} \right) \left( R_{12} + \frac{R_{13}}{2} \right) S_{12} - \frac{\Omega}{6} \right\} \Lambda \right], \quad (57)$$

$$q_{s,23}^{(0)} = -\frac{6}{K^3}(E_x \sin\theta \cos\phi + E_z \cos\theta) \Lambda \left[ (K^3 - 2\xi) \left( R_{12} + \frac{R_{13}}{2} \right) S_{12} - \frac{3S_{13}R_{12}K^3}{2} \right]. \quad (58)$$

Next, we proceed toward determining the leading-order velocity distribution using the boundary conditions Eqs. (17)–(20). These boundary conditions cannot be directly applied in terms of the growing and decaying solid spherical harmonics and therefore, we perform vectorial operations to transform the boundary conditions into simpler forms. The details of this procedure are provided in Refs. [46,52]. This yields a set of linear equations in terms of solid spherical harmonics which are solved to obtain the coefficients  $A_{n,m}^{(0)(i)}$ ,  $\hat{A}_{n,m}^{(0)(i)}$ ,  $A_{-n-1,m}^{(0)(i)}$ ,  $\hat{A}_{-n-1,m}^{(0)(i)}$ ,  $B_{n,m}^{(0)(i)}$ ,  $\hat{B}_{n,m}^{(0)(i)}$ ,  $B_{-n-1,m}^{(0)(i)}$ ,  $\hat{B}_{-n-1,m}^{(0)(i)}$ ,  $C_{n,m}^{(0)(i)}$ ,  $\hat{C}_{n,m}^{(0)(i)}$ ,  $C_{-n-1,m}^{(0)(i)}$ , and  $\hat{C}_{-n-1,m}^{(0)(i)}$ . However, in compact form, we represent the solution for the velocity and pressure distributions within the core and shell regions and outside the compound drop in terms of spherical harmonics as given in Appendix C.

Once the velocity and pressure distributions inside and outside the drop are obtained, we can determine the velocities of shell drop ( $U_2$ ) and core drop ( $U_3$ ), using the force-free condition [47,53]. The force-free condition at leading order in nondimensional form can be written as

$$\nabla(r^3 p_{-2}^{(0)(i)}) = 0, \quad (59)$$

where  $p_{-2}^{(0)(i)} = 1/r^2[A_{-2,0}^{(0)(i)}P_{1,0} + A_{-2,1}^{(0)(i)}\cos\phi P_{1,1} + \hat{A}_{-2,1}^{(0)(i)}\sin\phi P_{1,1}]$  with  $i = 2, 3$ . Solving Eq. (59) will yield leading-order velocities for the shell and core of the compound drop as

$$U_{2,x}^{(0)} = U_{2,y}^{(0)} = 0, \quad U_{2,z}^{(0)} = f(K, \lambda_{12}, \lambda_{13}, x_d), \quad (60)$$

$$U_{3,x}^{(0)} = U_{3,y}^{(0)} = 0, \quad U_{3,z}^{(0)} = f(K, \lambda_{12}, \lambda_{13}, x_d). \quad (61)$$

The leading-order normal stress balance condition Eq. (21) would then be utilized to determine the deformed shape of the compound drop. This provides nonzero coefficients ( $L_{n,m}^{(\text{Ca})(ij)}$ ) required to represent the  $O(\text{Ca})$  shape correction factor ( $f_{ij}^{(\text{Ca})}$ ) of the deformed  $ij$ th interface of the compound drop.

### 6. $O(\text{Re}_E)$ solution

Toward obtaining the  $O(\text{Re}_E)$  solution, we first expand the term  $[-\nabla_s \cdot (q_{s,ij}^{(0)} \mathbf{V}_{s,ij}^{(0)})]$  present in the boundary condition Eq. (25) as [54]

$$\begin{aligned} \nabla_s \cdot (q_{s,ij}^{(0)} \mathbf{V}_{s,ij}^{(0)}) &= 2 (q_{s,ij}^{(0)} \mathbf{V}_{s,ij}^{(0)} \cdot \mathbf{e}_r) + \frac{1}{\sin\theta} \frac{\partial}{\partial\theta} (\sin\theta q_{s,ij}^{(0)} \mathbf{V}_{s,ij}^{(0)} \cdot \mathbf{e}_\theta) + \frac{1}{\sin\theta} \frac{\partial}{\partial\phi} (q_{s,ij}^{(0)} \mathbf{V}_{s,ij}^{(0)} \cdot \mathbf{e}_\phi) \\ &= \sum_{n=0}^{\infty} \sum_{m=0}^n [Z_{n,m} \cos(m\phi) + \hat{Z}_{n,m} \sin(m\phi)] P_{n,m}(\cos\theta), \end{aligned} \quad (62)$$

where  $q_{s,ij}^{(0)}$  and  $\mathbf{V}_{s,ij}^{(0)}$  ( $\mathbf{V}_{s,12}^{(0)} = \mathbf{u}_2^{(0)}$  and  $\mathbf{V}_{s,23}^{(0)} = \mathbf{u}_3^{(0)}$ ) are substituted from Eqs. (57), (58), and Eqs. (C3)–(C5). Applying the orthogonality property of spherical surface harmonics, we find out the nonzero  $Z_{n,m}$  and  $\hat{Z}_{n,m}$  terms. Based on these nonzero terms, it is expected that the electric potential in the suspending medium, i.e., the shell and core drops, governs by the expression given in Appendix D.

Thereafter, we utilize the boundary conditions Eqs. (23)–(25) and determine the coefficients  $a_{-n-1,m}^{(\text{Re}_E)}$ ,  $\hat{a}_{-n-1,m}^{(\text{Re}_E)}$ ,  $b_{n,m}^{(\text{Re}_E)}$ ,  $\hat{b}_{n,m}^{(\text{Re}_E)}$ ,  $b_{-n-1,m}^{(\text{Re}_E)}$ ,  $\hat{b}_{-n-1,m}^{(\text{Re}_E)}$ ,  $c_{n,m}^{(\text{Re}_E)}$ , and  $\hat{c}_{n,m}^{(\text{Re}_E)}$  that have nonzero values and hence determine the  $O(\text{Re}_E)$  surface charge density.

In a similar way as the leading-order case, the force-free condition at  $O(\text{Re}_E)$  takes the form

$$\nabla(r^3 p_{-2}^{(\text{Re}_E)(i)}) = 0, \quad (63)$$

where  $p_{-2}^{(\text{Re}_E)(i)} = 1/r^2[A_{-2,0}^{(\text{Re}_E)(i)}P_{1,0} + A_{-2,1}^{(\text{Re}_E)(i)}\cos\phi P_{1,1} + \hat{A}_{-2,1}^{(\text{Re}_E)(i)}\sin\phi P_{1,1}]$  with  $i = 2, 3$ . Using the expression for  $p_{-2}^{(\text{Re}_E)(i)}$ , we determine the nonzero expressions for the coefficients  $A_{-2,0}^{(\text{Re}_E)(i)}$ ,  $A_{-2,1}^{(\text{Re}_E)(i)}$  and  $\hat{A}_{-2,1}^{(\text{Re}_E)(i)}$ . Thereafter, we employ Eq. (70) and evaluate the  $O(\text{Re}_E)$  velocities for shell and core drops in the following form:

$$U_{2,x}^{(\text{Re}_E)} = U_{2,z}^{(\text{Re}_E)} = f(K, \lambda_{12}, \lambda_{13}, R_{12}, R_{13}, S_{12}, S_{13}, \theta_t, x_d), \quad U_{2,y}^{(\text{Re}_E)} = 0, \quad (64)$$

$$U_{3,x}^{(\text{Re}_E)} = U_{3,z}^{(\text{Re}_E)} = f(K, \lambda_{12}, \lambda_{13}, R_{12}, R_{13}, S_{12}, S_{13}, \theta_t, x_d), \quad U_{3,y}^{(\text{Re}_E)} = 0. \quad (65)$$

It is to be noted, however, that by considering a uniform background flow, the charge convection will not affect the drop velocity in  $O(\text{Re}_E)$ , and this has been mathematically shown in Appendix E.



### 7. $O(\text{Ca})$ solution

As the boundary conditions for  $O(\text{Ca})$  are applied at the deformed interface ( $\mathbf{r} = K_i + \text{Ca} f_{ij}^{(\text{Ca})}$ ) and there is no applied electric field, hence shape deformation of the compound drop is responsible for the induced electric field at this order. The nonzero harmonics are obtained using the boundary conditions Eqs. (33)–(35). The expressions for the electric potential for  $O(\text{Ca})$  are given in Appendix F.

The evaluation of the  $O(\text{Ca})$  velocity and pressure fields are rather cumbersome as the quantities are to be determined at the deformed interfaces ( $\mathbf{r} = K_i + \text{Ca} f_{ij}^{(\text{Ca})}$ ) of the compound drop and details of this procedure can be found in Refs. [52,53]. Briefly stating, we employ the force-free condition

$$\nabla(r^3 p_{-2}^{(\text{Ca})(i)}) = 0, \quad (66)$$

where  $p_{-2}^{(\text{Ca})(i)} = 1/r^2 [A_{-2,0}^{(\text{Ca})(i)} P_{1,0} + A_{-2,1}^{(\text{Ca})(i)} \cos\phi P_{1,1} + \hat{A}_{-2,1}^{(\text{Ca})(i)} \sin\phi P_{1,1}]$  with  $i = 2, 3$ . We solve the expression for  $p_{-2}^{(\text{Ca})(i)}$  to determine the nonzero expressions for the coefficients  $A_{-2,0}^{(\text{Ca})(i)}$ ,  $A_{-2,1}^{(\text{Ca})(i)}$ , and  $\hat{A}_{-2,1}^{(\text{Ca})(i)}$ . Following the procedure given in Refs. [52,53], we arrive at the  $O(\text{Ca})$  velocities for shell and core regions of the compound drop, which are given by

$$U_{2,x}^{(\text{Ca})} = U_{2,z}^{(\text{Ca})} = f(K, \lambda_{12}, \lambda_{13}, R_{12}, R_{13}, S_{12}, S_{13}, \theta_t, x_d), \quad U_{2,y}^{(\text{Ca})} = 0, \quad (67)$$

$$U_{3,x}^{(\text{Ca})} = U_{3,z}^{(\text{Ca})} = f(K, \lambda_{12}, \lambda_{13}, R_{12}, R_{13}, S_{12}, S_{13}, \theta_t, x_d), \quad U_{3,y}^{(\text{Ca})} = 0. \quad (68)$$

Finally, the combined effect of charge convection and shape deformation on the velocity of the shell and core phases can be obtained by combining these two effects linearly as

$$\mathbf{U}_i = \mathbf{U}_i^{(0)} + \text{Re}_E \mathbf{U}_i^{(\text{Re}_E)} + \text{Ca} \mathbf{U}_i^{(\text{Ca})}. \quad (69)$$

The solution obtained using the above formulation has been validated with that of Taylor [1], Santra *et al.* [43], and Chan and Leal [48], which is discussed in Appendix G.

### E. Leading-order analysis for eccentric compound drop

A schematic representation of the eccentric compound drop configuration is shown in Fig. 2. A bispherical coordinate system  $(\xi, \eta, \varphi)$  with the origin as shown in the figure is considered. The interfaces of outer and inner drops are expressed in bispherical coordinates as  $\xi = \xi_1 = \cosh^{-1}(\frac{1+e^2-K^2}{2e})$  and  $\xi = \xi_2 = \cosh^{-1}(\frac{1-e^2-K^2}{2eK})$ , respectively. Here,  $e$  represents the eccentricity of the compound drop. The reference cylindrical coordinate system is related to the bispherical coordinate system as follows [55]:

$$\rho = \frac{c\sqrt{1-\zeta^2}}{\cosh\xi - \zeta}, \quad z = \frac{c \sinh\xi}{\cosh\xi - \zeta}, \quad \varphi = \varphi, \quad (70)$$

where  $\zeta = \cos\eta$  and  $c = K \sinh\xi_1$ .

Following the irrotational nature of the electric field intensity ( $\nabla \times \mathbf{E}_i = 0$ ), the electrostatic problem can be reformulated by defining a scalar function  $\omega$ , which is related to an electric field intensity as follows [56]:

$$\mathbf{E}_i = -\nabla\psi_i = \nabla \times \left( \frac{\omega_i}{\rho} \hat{\mathbf{i}}_\varphi \right). \quad (71)$$

As a result, Eq. (71) trivially satisfies the governing equation for electric potential [Eq. (12)]. Therefore, Eq. (71) in combination with  $\nabla \times \mathbf{E}_i = 0$  yields the governing equation for  $\omega$  as

$$\nabla \times \nabla \times \left( \frac{\omega_i}{\rho} \right) \hat{\mathbf{i}}_\varphi = 0, \quad (72)$$

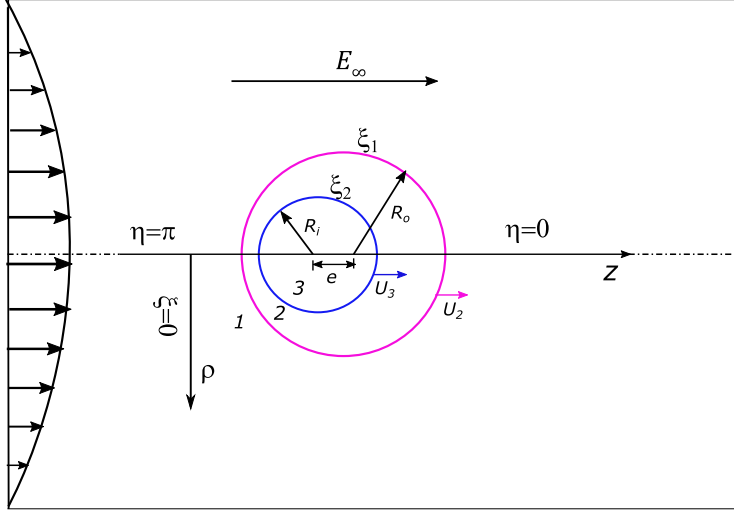


FIG. 2. A schematic representation of eccentric compound drop configuration moving under the action of background Poiseuille flow and subjected to an imposed external electric field applied in the direction of flow. A bispherical coordinate system  $(\xi, \eta, \varphi)$  is considered. The interfaces of outer and inner drops are expressed in bispherical coordinates as  $\xi = \xi_1$  and  $\xi = \xi_2$ , respectively. Here,  $e$  represents the eccentricity of the compound drop.

where the gradient operator  $(\nabla)$  takes the form [57]  $\nabla = \hat{i}_\eta h_1 \partial / \partial \eta + \hat{i}_\xi h_2 \partial / \partial \xi + \hat{i}_\varphi h_3 \partial / \partial \varphi$  with  $h_1 = h_2 = (\cosh \xi - \zeta) / c$  and  $h_3 = (\cosh \xi - \zeta) / (c \sqrt{1 - \zeta^2})$ . Further simplification of Eq. (72) yields  $\varepsilon^2 \omega_i = 0$ , where  $\varepsilon^2$  in bispherical coordinates is given by [58]

$$\varepsilon^2 \equiv \frac{(\cosh \xi - \zeta)}{c^2} \left[ \frac{\partial}{\partial \xi} \left\{ (\cosh \xi - \zeta) \frac{\partial}{\partial \xi} \right\} + (1 - \zeta^2) \frac{\partial}{\partial \zeta} \left\{ (\cosh \xi - \zeta) \frac{\partial}{\partial \zeta} \right\} \right]. \quad (73)$$

The general solution for  $\omega$  can be expressed as [59]

$$\omega = (\cosh \xi - \zeta)^{-\frac{1}{2}} \sum_{n=0}^{\infty} \left[ d_n \cosh \left( n + \frac{1}{2} \right) \xi + e_n \sinh \left( n + \frac{1}{2} \right) \xi \right] C_{n+1}^{-\frac{1}{2}}(\zeta), \quad (74)$$

where  $C_{n+1}^{-\frac{1}{2}}$  is the Gegenbauer polynomial of degree  $-1/2$  and order  $(n+1)$ . Based on the boundary conditions for the electric potential at the leading order, we choose suitable forms of  $\omega_i$  for the  $i$ th fluid as follows [60]:

$$\omega_1 = \frac{\rho^2}{2} + (\cosh \xi - \zeta)^{-\frac{1}{2}} \sum_{n=0}^{\infty} \left[ d_n \sinh \left( n + \frac{1}{2} \right) \xi \right] C_{n+1}^{-\frac{1}{2}}(\zeta), \quad (75)$$

$$\omega_2 = (\cosh \xi - \zeta)^{-\frac{1}{2}} \sum_{n=0}^{\infty} [f_n e^{(n+\frac{1}{2})(\xi-\xi_2)} + g_n e^{-(n+\frac{1}{2})(\xi-\xi_2)}] C_{n+1}^{-\frac{1}{2}}(\zeta), \quad (76)$$

$$\omega_3 = (\cosh \xi - \zeta)^{-\frac{1}{2}} \sum_{n=0}^{\infty} [h_n e^{\mp(n+\frac{1}{2})(\xi-\xi_2)}] C_{n+1}^{-\frac{1}{2}}(\zeta). \quad (77)$$

It is to be noted that the above forms of  $\omega_i$  are chosen because they satisfy the leading-order far-field condition ( $\omega_1 \rightarrow \rho^2/2$ , as  $\xi, \eta \rightarrow 0$ ) and the boundedness condition ( $|\omega_3| < \infty$ , as  $\xi \rightarrow \infty$ ) in

bispherical coordinates [60]. The remaining boundary conditions [Eqs. (14) and (15)] will take the following form [33]:

$$\left. \frac{\partial \omega_i}{\partial \xi} \right|_{\xi=\xi_i} = \left. \frac{\partial \omega_j}{\partial \xi} \right|_{\xi=\xi_i}, \quad (78)$$

$$R_{1i}\omega_i|_{\xi=\xi_i} = R_{1j}\omega_j|_{\xi=\xi_i}. \quad (79)$$

To proceed with the solution of potential field, we need to transform the boundary conditions Eqs. (78) and (79) into a set of linear algebraic equations using Eqs. (75)–(77), the orthogonality property of Gegenbauer polynomial, the recurrence relations and a few well-known identities as given in Jadhav and Ghosh [61]. This results in the equations given in Appendix I that can be solved numerically for the unknown coefficients ( $d_n$ ,  $f_n$ ,  $g_n$ , and  $h_n$  for  $0 \leq n \leq N$ ). Here,  $N$  is the total number of terms in the series and it is chosen to truncate the series after  $N$  terms. For the sake of accuracy in results, the choice of  $N$  is dependent on the value of eccentricity of the compound drop. Further details of the numerical solution procedure of Eqs. (12)–(15) is given in Jadhav and Ghosh [61]. Once the unknown coefficients and hence  $\omega_i$  are obtained, it can be related to the gradient of electric potential through the following relations:

$$E_\xi^{(i)} = -\frac{(\cosh \xi - \zeta)}{c} \frac{\partial \psi_i}{\partial \xi} = \frac{(\cosh \xi - \zeta)^2}{c^2 \sin \eta} \frac{\partial \omega_i}{\partial \eta}, \quad (80)$$

$$E_\eta^{(i)} = -\frac{(\cosh \xi - \zeta)}{c} \frac{\partial \psi_i}{\partial \eta} = -\frac{(\cosh \xi - \zeta)^2}{c^2 \sin \eta} \frac{\partial \omega_i}{\partial \xi}. \quad (81)$$

Having solved for the electric potential field, we can now proceed toward solving the flow field considering a special case of axisymmetric flow for the eccentric compound drop system subjected to plane Poiseuille flow. This allows us to write the governing equation for the flow field of the  $i$ th fluid as [57]  $\varepsilon^4 S_i = 0$ , where  $S_i$  is the Stokes stream function for the  $i$ th fluid and the general solution for the same in bispherical coordinates can be expressed as [58]

$$S_i = (\cosh \xi - \zeta)^{-\frac{3}{2}} \sum_{n=0}^{\infty} \Xi_n^{(i)}(\xi) C_{n+1}^{-\frac{1}{2}}(\zeta). \quad (82)$$

In Eq. (82), depending on the satisfaction of far-field and boundedness condition,  $\Xi_n^{(i)}$  will assume suitable forms as follows [44]:

$$\Xi_n^{(1)} = D_n e^{(n-\frac{1}{2})\xi} + E_n e^{(n+\frac{3}{2})\xi} + \tilde{f}_n e^{\mp(n-\frac{1}{2})\xi} + \tilde{g}_n e^{\mp(n+\frac{3}{2})\xi}, \quad (83)$$

$$\Xi_n^{(2)} = H_n e^{(n-\frac{1}{2})\xi} + I_n e^{(n+\frac{3}{2})\xi} + J_n e^{\mp(n-\frac{1}{2})\xi} + K_n e^{\mp(n+\frac{3}{2})\xi}, \quad (84)$$

$$\Xi_n^{(3)} = L_n e^{\mp(n-\frac{1}{2})\xi} + M_n e^{\mp(n+\frac{3}{2})\xi}. \quad (85)$$

Using the relations between the velocity components ( $u_\xi$  and  $u_\eta$ ) and the stream function as follows [44]:

$$u_\xi^{(i)} = \frac{(\cosh \xi - \zeta)^2}{c^2 \sin \eta} \frac{\partial S_i}{\partial \eta} \quad \text{and} \quad u_\eta^{(i)} = -\frac{(\cosh \xi - \zeta)^2}{c^2 \sin \eta} \frac{\partial S_i}{\partial \xi}. \quad (86)$$

We can recast the leading-order far-field condition [Eq. (17)] in the following form [44]:

$$S_1 = (\cosh \xi - \zeta)^{-\frac{3}{2}} \sum_{n=0}^{\infty} [\tilde{f}_n e^{\mp(n-\frac{1}{2})\xi} + \tilde{g}_n e^{\mp(n+\frac{3}{2})\xi}] C_{n+1}^{-\frac{1}{2}}(\zeta) \quad \text{as } \xi \rightarrow 0. \quad (87)$$

Here, the constants  $\tilde{f}_n$  and  $\tilde{g}_n$  can be expressed as [44]

$$\tilde{f}_n = -\frac{n(n+1)c^2}{\sqrt{2}(2n-1)} \left[ (1-U_2) + \frac{2c^2}{3R^2}(n-1)(n-2) \right], \quad (88)$$

$$\tilde{g}_n = \frac{n(n+1)c^2}{\sqrt{2}(2n+3)} \left[ (1-U_2) + \frac{2c^2}{3R^2}(n+2)(n+3) \right]. \quad (89)$$

We now recast the leading-order boundary conditions for the flow field [refer to Eqs. (18)–(20)] as per the bispherical coordinate system at the interface ( $\xi = \xi_i$ ) as follows [33]:

$$u_\xi^{(i)} = u_\xi^{(j)} = \delta_{i2}(U_3 - U_2) \cdot \hat{i}_\xi, \quad (90)$$

$$u_\eta^{(i)} = u_\eta^{(j)}, \quad (91)$$

$$\lambda_i \tau_{\xi\eta}^{(i)} - \lambda_j \tau_{\xi\eta}^{(j)} = \frac{E_\eta^{(i)}}{4\pi} (S_{1j} E_\xi^{(j)} - S_{1i} E_\xi^{(i)}). \quad (92)$$

Using the expression for the shear stress component in bispherical coordinates and the orthogonality property of the Gegenbauer polynomial, we can transform the boundary conditions Eqs. (90)–(92) into a set of eight linear algebraic equations as given in Appendix J. These equations contain eight unknowns ( $D_n, E_n, H_n, I_n, J_n, K_n, L_n, M_n$ ) and they can be found out for each mode  $n$  using appropriate numerical technique. For simplicity, we consider the number of modes for the flow field to be the same as that considered for the potential field, i.e.,  $n = N$ . Once the values of the unknown coefficients in the flow field are determined, they can be individually expressed as a linear combination of the shell and core drop velocities in the following way [44]:

$$\Theta_n = \vartheta_1^{(i)}[\Pi, e(t); n] + \vartheta_2^{(i)}[\Pi, e(t); n]U_2 + \vartheta_3^{(i)}[\Pi, e(t); n]U_3. \quad (93)$$

Here,  $\Theta = [D, E, H, I, J, K, L, M]$  and  $\Pi$  is the parameter matrix which includes  $\lambda_{12}, \lambda_{13}, R_{12}, R_{13}, S_{12}, S_{13}$ , and  $K$ . Using an overall force balance equation as follows:

$$F_{\text{shell}} = \frac{4\sqrt{2}\pi}{c} \sum_{n=0}^{\infty} (D_n + E_n) = 0, \quad (94)$$

$$F_{\text{core}} = \frac{4\sqrt{2}\pi}{c} \sum_{n=0}^{\infty} (H_n + I_n) = 0. \quad (95)$$

Now we deduce two independent linear equations for  $U_2$  and  $U_3$  in the following form [31]:

$$\aleph_{21}U_2 + \aleph_{31}U_3 + \aleph_1 = 0, \quad (96)$$

$$\aleph_{22}U_2 + \aleph_{32}U_3 + \aleph_2 = 0, \quad (97)$$

where,  $\aleph_{21} = \sum_{n=0}^N (\vartheta_2^{(1)} + \vartheta_2^{(2)})$ ,  $\aleph_{31} = \sum_{n=0}^N (\vartheta_3^{(1)} + \vartheta_3^{(2)})$ ,  $\aleph_1 = \sum_{n=0}^N (\vartheta_1^{(1)} + \vartheta_1^{(2)})$ , and so on. Equations (96) and (97) can be easily solved to determine the shell and core drop velocities.

### III. RESULTS AND DISCUSSION

In this section, first, the dynamics of an undeformed concentric compound drop is discussed, followed by the dynamics of a deformed concentric compound drop. Thereafter, the combined effect of charge convection and shape deformation on the concentric compound drop is examined. Finally, a brief discussion on eccentric compound drop under plane Poiseuille flow and subjected to an electric field is also presented.

## A. Undeformed concentric compound drop

### 1. Interfacial charge distribution

We begin the presentation of our results by analyzing the charge distribution on the surface of the shell and core regions of the compound drop due to the changes in physical and electrohydrodynamic parameters. The distributions of charges on the surface of the shell and core of the compound drop are presented in Figs. 3 and 4, respectively. Following observations can be made from these results. First, it is seen from the plots in the first row of Fig. 3 that the antisymmetry in charge distribution on the surface of the shell drop is disturbed due to charge convection. The disturbance is maximum when the tilt angle of the applied electric field is  $\pi/4$  as in this case the charge distribution becomes asymmetric about both the axial and transverse planes. However, the antisymmetry in the distribution of charges on the surface of the core drop is disturbed (refer to the plots in the first row of Fig. 4) in terms of the magnitude of positive and negative charges. Also, the polarity of the charges on the surface of the shell drop is opposite to that on the surface of the core drop. In other words, if negative charges accumulate at the north pole of the shell drop then positive charges accumulate at the north pole of the core drop, irrespective of the tilt angle of the applied electric field. Second, the disturbance in the antisymmetric distribution of charges on the surface of the shell and core of the drop increases with the increase in the Mason number (refer to the plots in the second row of Figs. 3 and 4). Thirdly, the disturbance in the antisymmetric distribution of charges on the surface of the shell and core of the drop increases with the increase in electric Reynolds number (refer to the plots in the third row of Figs. 3 and 4). Lastly, with the increase in radius ratio of the compound drop, the disturbance in the antisymmetric distribution of charges on the surface of the shell and the core of the drop also increases (refer to the plots in the fourth row of Figs. 3 and 4). Moreover, the magnitude of charges on the surface of the core drop increases as the radius ratio of the compound drop is increased.

To investigate the quantitative variation of surface charge density, we plot the polar variation of the surface charges on the surface of the shell and core of the drop at two symmetrically opposite locations about the axial plane ( $\phi = \pi/4$  and  $\phi = 3\pi/4$ ) and also for three different radius ratio of the compound drop ( $K = 0.3, 0.5, \text{ and } 0.7$ ) considering the effect of charge convection in Figs. 5(a) and 5(b). In this plot, the initial center of the compound drop is placed at an off-center location (i.e.,  $x_d = 4$ ) and the rest of the parameters are provided in the figure caption. It is clear from this figure that the charge distribution on the surface of the shell and core of the drop are asymmetric about the transverse plane ( $\theta = \pi/2$  plane) for both the values of  $\phi$  under consideration. Consequently, the asymmetric distribution in surface charge density about the transverse plane leads to an asymmetric distribution of tangential electric force on the surface of the shell and core of the drop as evident from Figs. 5(c) and 5(d). Another important aspect that can be drawn from Fig. 5 is that the magnitude of surface charge density (thus, the tangential electric force) increases with the increase in the radius ratio of the compound drop. Additionally, the asymmetry in the charge distribution on the shell and core surfaces about the transverse plane is also increased with the increase in radius ratio of the compound drop.

### 2. Velocity in the cross-stream direction

Mandal *et al.* [44] showed that for a nondeformable single drop, the charge convection effect can lead to considerable asymmetry in surface charge distribution about the axial plane that results in nonzero velocity  $O(\text{Re}_E)$  in the transverse direction. Even in the case of compound drop (as discussed in the previous section), the difference in the asymmetry of surface charge distribution is observed for  $\phi = \pi/4$  and  $\phi = 3\pi/4$ . This points to a critical alteration in velocity in the transverse direction, and therefore, we investigate the variation of  $U_{2,x}^{(\text{Re}_E)}$  and  $U_{3,x}^{(\text{Re}_E)}$  with  $\lambda_{12}$  in Fig. 6 for different values of  $K$ . For conditions when the viscosity of the fluid in the shell drop is very much less than the viscosity of the suspending medium, i.e.,  $\lambda_{12} \ll 1$ , the compound drop arrangement resembles the behavior of a bubble encompassing a drop. As a result, the retardation due to charge convection is maximum for both the shell and the core of the drop in such a situation. However,

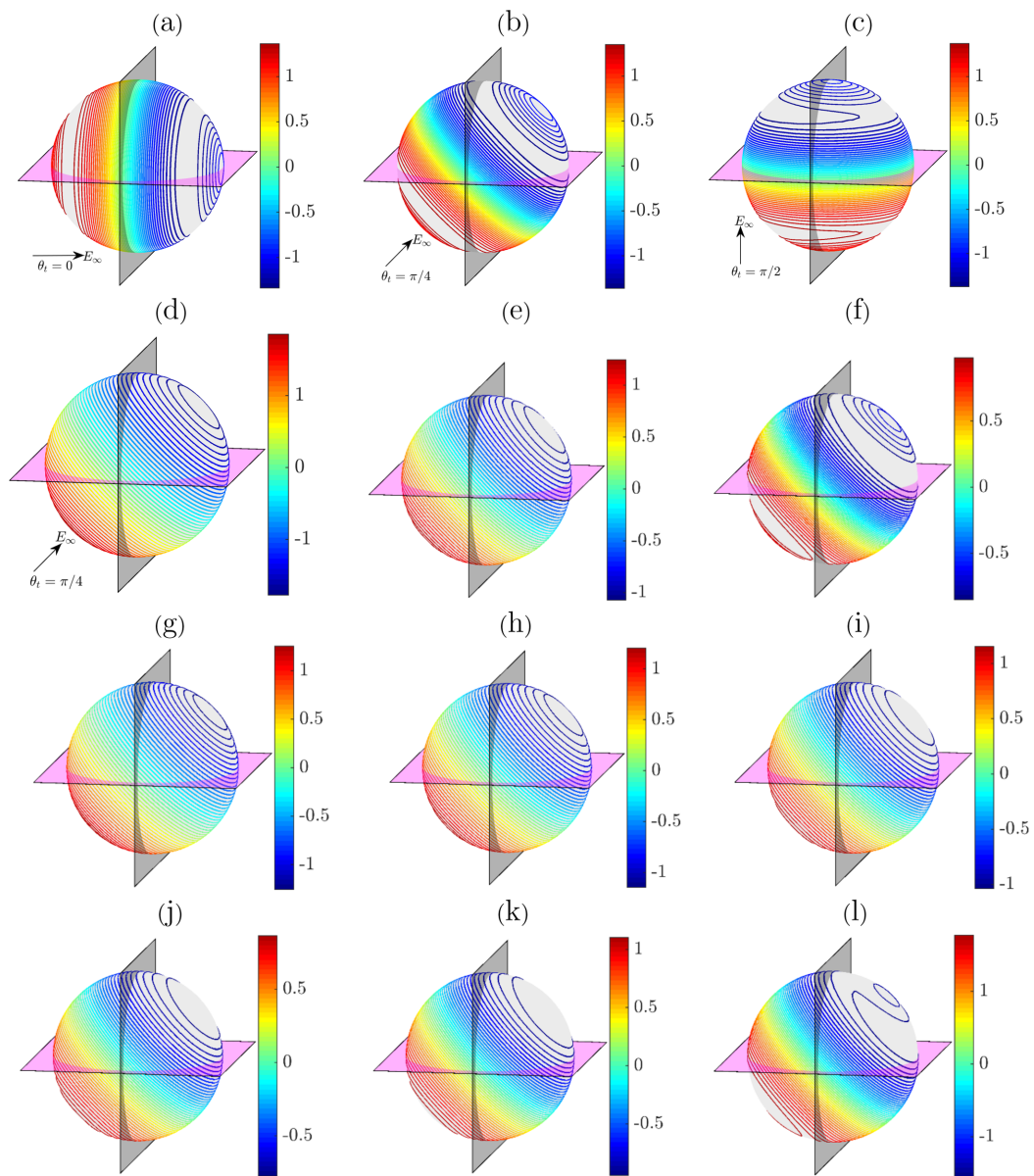


FIG. 3. The surface charge distribution ( $q_{s,12}^{(0)} + \text{Re}_E q_{s,12}^{(\text{Re}_E)}$ ) at the shell drop surface for different values of tilt angle of the applied electric field ( $\theta_t$ ), Mason number ( $M$ ), electric Reynolds number ( $\text{Re}_E$ ), and radius ratio of the concentric compound drop ( $K$ ). In panels (a)–(c)  $\theta_t$  is varied with  $M = 1$ ,  $\text{Re}_E = 0.3$ ,  $K = 0.5$ : (a)  $\theta_t = 0$ , (b)  $\theta_t = \frac{\pi}{4}$ , (c)  $\theta_t = \frac{\pi}{2}$ . In panels (d)–(f)  $M$  is varied with  $\theta_t = \frac{\pi}{4}$ ,  $\text{Re}_E = 0.3$ ,  $K = 0.5$ : (d)  $M = 0.1$ , (e)  $M = 0.5$ , (f)  $M = 2$ . In panels (g)–(i)  $\text{Re}_E$  is varied with  $\theta_t = \frac{\pi}{4}$ ,  $M = 1$ ,  $K = 0.5$ : (g)  $\text{Re}_E = 0$ , (h)  $\text{Re}_E = 0.1$ , (i)  $\text{Re}_E = 0.2$ . In panels (j)–(l)  $K$  is varied with  $\theta_t = \frac{\pi}{4}$ ,  $M = 1$ ,  $\text{Re}_E = 0.3$ : (j)  $K = 0.3$ , (k)  $K = 0.5$ , (l)  $K = 0.7$ . The rest of the parameters are  $R_{12} = 0.01$ ,  $R_{13} = 1$ ,  $S_{12} = 0.63$ ,  $S_{13} = 1$ ,  $\lambda_{12} = 0.35$ ,  $\lambda_{13} = 1$ ,  $H = 10$ , and  $x_d = 4$ . Colorbar represents the magnitude of the dimensionless surface charge density.



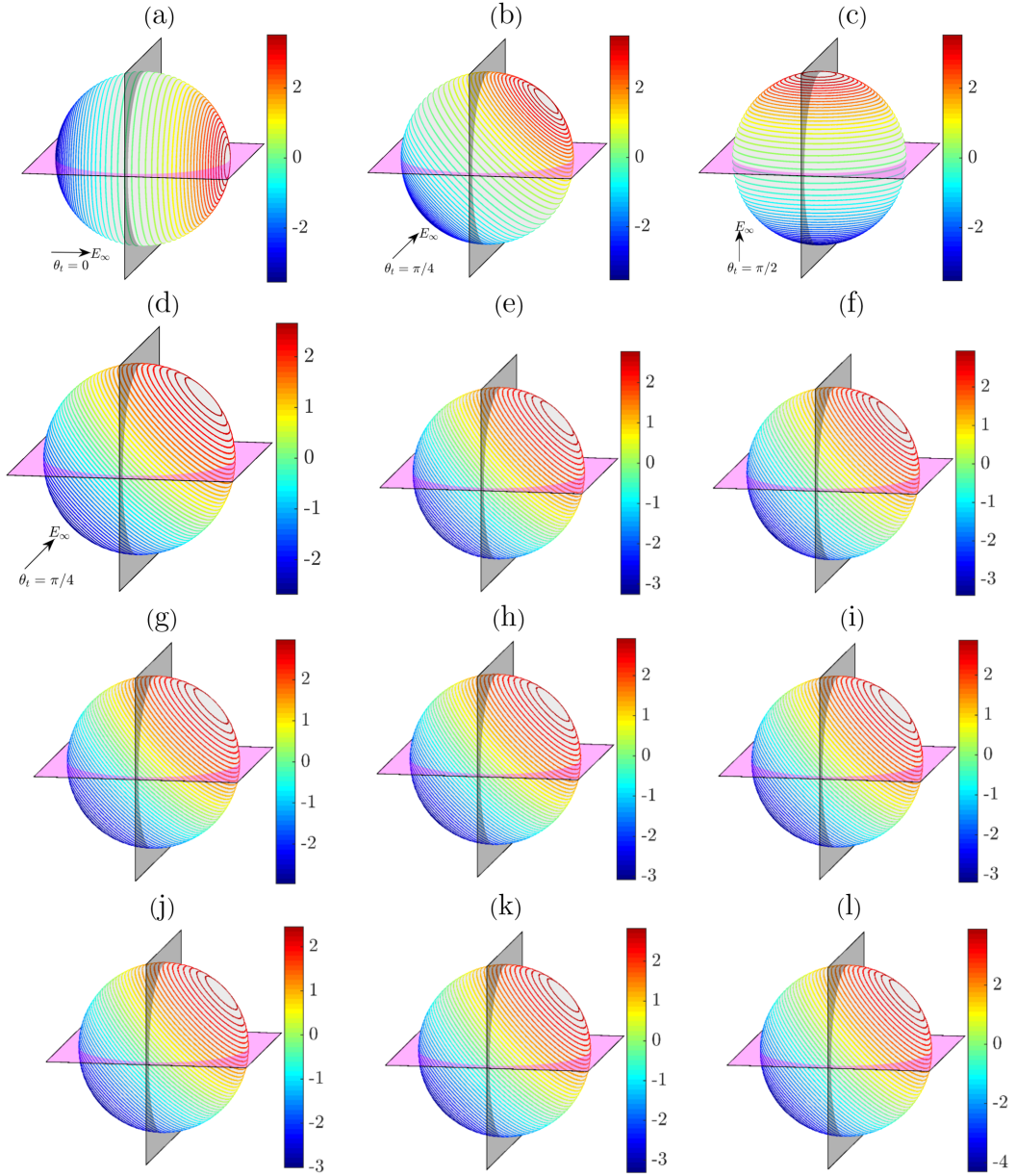


FIG. 4. The surface charge distribution ( $q_{s,23}^{(0)} + \text{Re}_E q_{s,23}^{(\text{Re}_E)}$ ) at the surface of the core drop for different values of tilt angle of the applied electric field ( $\theta_t$ ), Mason number ( $M$ ), electric Reynolds number ( $\text{Re}_E$ ), and radius ratio of the concentric compound drop ( $K$ ). In panels (a)–(c)  $\theta_t$  is varied with  $M = 1$ ,  $\text{Re}_E = 0.3$ ,  $K = 0.5$ : (a)  $\theta_t = 0$ , (b)  $\theta_t = \frac{\pi}{4}$ , (c)  $\theta_t = \frac{\pi}{2}$ . In panels (d)–(f)  $M$  is varied with  $\theta_t = \frac{\pi}{4}$ ,  $\text{Re}_E = 0.3$ ,  $K = 0.5$ : (d)  $M = 0.1$ , (e)  $M = 0.5$ , (f)  $M = 2$ . In panels (g)–(i)  $\text{Re}_E$  is varied with  $\theta_t = \frac{\pi}{4}$ ,  $M = 1$ ,  $K = 0.5$ : (g)  $\text{Re}_E = 0$ , (h)  $\text{Re}_E = 0.1$ , (i)  $\text{Re}_E = 0.2$ . In panels (j)–(l)  $K$  is varied with  $\theta_t = \frac{\pi}{4}$ ,  $M = 1$ ,  $\text{Re}_E = 0.3$ : (j)  $K = 0.3$ , (k)  $K = 0.5$ , (l)  $K = 0.7$ . The rest of the parameters are  $R_{12} = 0.01$ ,  $R_{13} = 1$ ,  $S_{12} = 0.63$ ,  $S_{13} = 1$ ,  $\lambda_{12} = 0.35$ ,  $\lambda_{13} = 1$ ,  $H = 10$ , and  $x_d = 4$ . Colorbar represents the magnitude of the dimensionless surface charge density.

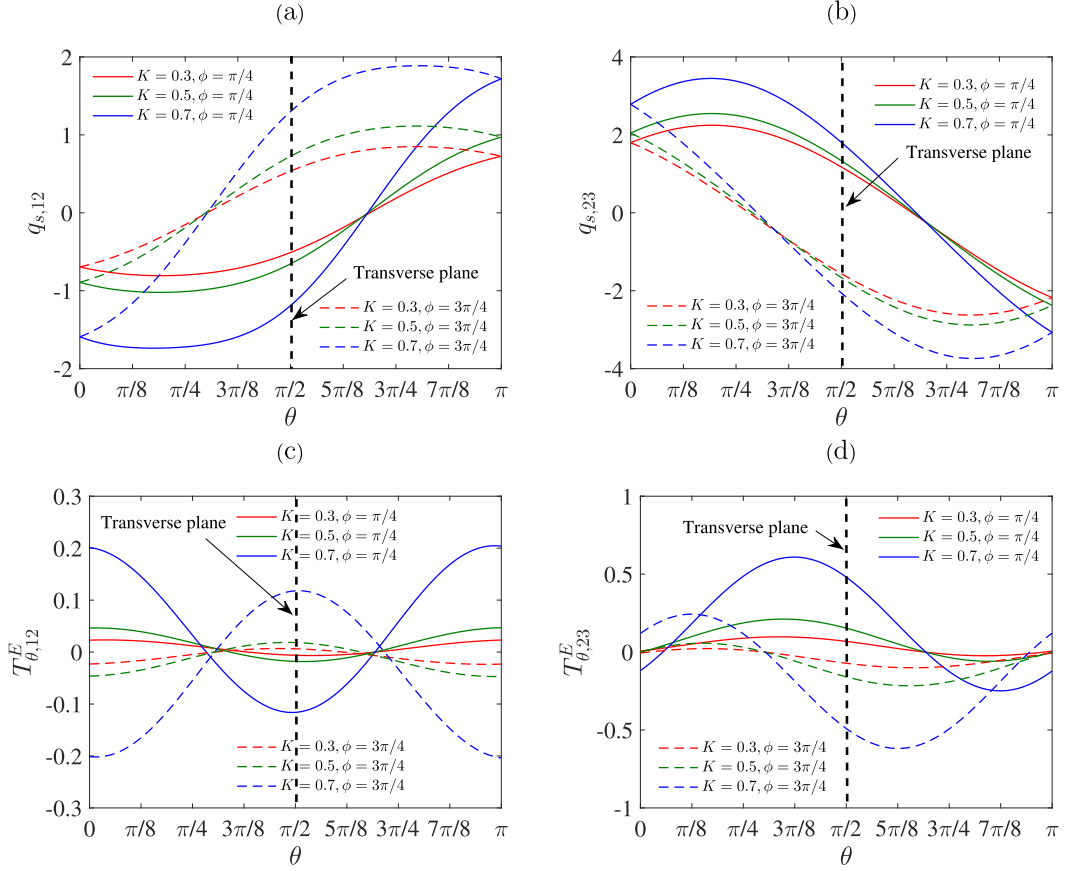


FIG. 5. Variation of (a)  $q_{s,12}(\theta)$ , (b)  $q_{s,23}(\theta)$ , (c)  $T_{\theta,12}^E(\theta)$ , and (d)  $T_{\theta,23}^E(\theta)$  for  $\phi = \pi/4$  and  $3\pi/4$  and for different values of  $K$ . The rest of the parameters are  $R_{12} = 0.01$ ,  $R_{13} = 1$ ,  $S_{12} = 0.63$ ,  $S_{13} = 1$ ,  $\lambda_{12} = 0.35$ ,  $\lambda_{13} = 1$ ,  $M = 1$ ,  $\text{Re}_E = 0.2$ ,  $H = 10$ , and  $x_d = 4$ .

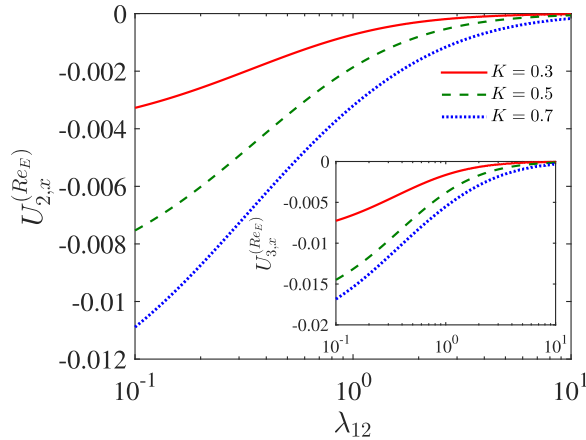


FIG. 6. Variation of the lateral velocity due to charge convection  $U_{2,x}^{(\text{Re}_E)}$  and  $U_{3,x}^{(\text{Re}_E)}$  (shown in the inset) with change in  $\lambda_{12}$  for different values of  $K$ . The rest of the parameters are  $R_{12} = 0.01$ ,  $R_{13} = 1$ ,  $S_{12} = 0.63$ ,  $S_{13} = 1$ ,  $\lambda_{13} = 1$ ,  $\theta_t = \pi/4$ ,  $M = 0.1$ ,  $H = 10$ , and  $x_d = 4$ .

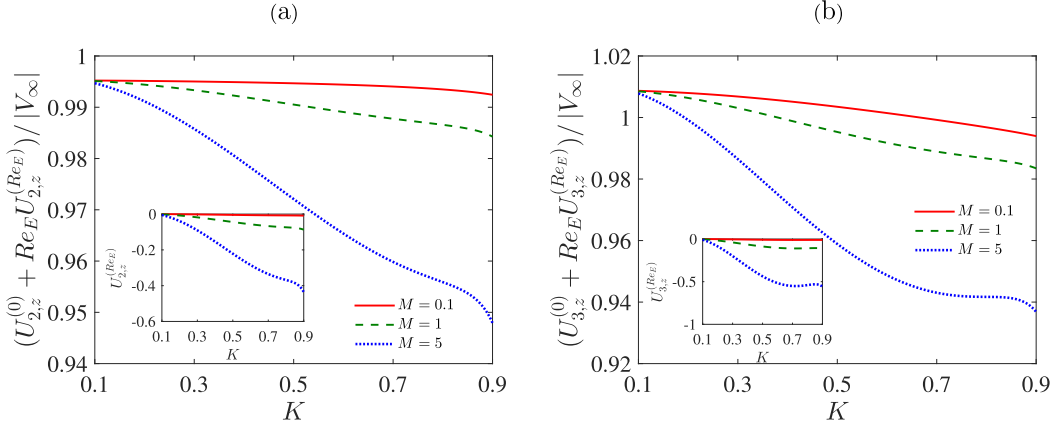


FIG. 7. Variation of the longitudinal velocity due to charge convection. Variations of (a)  $(U_{2,z}^{(0)} + \text{Re}_E U_{2,z}^{(\text{Re}_E)})/|V_\infty|$  and (b)  $(U_{3,z}^{(0)} + \text{Re}_E U_{3,z}^{(\text{Re}_E)})/|V_\infty|$  with change in  $K$  for different values of  $M$ . The rest of the parameters are  $R_{12} = 0.01$ ,  $R_{13} = 1$ ,  $S_{12} = 0.63$ ,  $S_{13} = 1$ ,  $\lambda_{12} = 0.35$ ,  $\lambda_{13} = 1$ ,  $\theta_t = \pi/4$ ,  $H = 10$  and  $x_d = 4$ . Here,  $|V_\infty| = 0.96$ .

the reverse is true for  $\lambda_{12} \gg 1$ , as in this case, the viscosity of the fluid in the shell drop is much higher than the viscosity of the suspending medium. Thus, the shell drop resembles the behavior of a rigid sphere, making the compound drop almost immobile. Also, the magnitude of the transverse component of velocity for both the shell and core drops being maximum for  $\lambda_{12} \ll 1$  and minimum for  $\lambda_{12} \gg 1$  can be directly related to the internal circulation strength. As the drop internal viscosity increases, the internal circulation strength becomes weaker, which in turn minimizes the intensity of charge convection and hence reduces the drop velocity. Additionally, when the radius ratio of the compound drop increases, the internal circulation strength and, as a result, the intensity of charge convection increases due to the reduced annular space. Thus, we can see an increment in the magnitude of  $U_{2,x}^{(\text{Re}_E)}$  and  $U_{3,x}^{(\text{Re}_E)}$  with the increase in  $K$ .

### 3. Velocity in the longitudinal direction

For a nondeformable drop, the component of velocity parallel to the direction of imposed flow, i.e.,  $z$  direction, is the summation of leading-order velocity and the velocity due to charge convection ( $U_{i,z}^{(0)} + \text{Re}_E U_{i,z}^{(\text{Re}_E)}$ ,  $i = 2, 3$ ). To further understand the effect of the electric field on the alteration of longitudinal drop velocity due to charge convection for a compound drop, we present the variation of  $U_{i,z}^{(0)} + \text{Re}_E U_{i,z}^{(\text{Re}_E)}$  for the shell ( $i = 2$ ) and core ( $i = 3$ ) drop relative to the imposed background flow ( $|V_\infty|$ ) owing to changes in  $K$  for different values of  $M$  in Figs. 7(a) and 7(b), respectively. The values of the rest of the parameters are provided in the caption of this figure. It can be observed that the value of  $[(U_{2,z}^{(0)} + \text{Re}_E U_{2,z}^{(\text{Re}_E)})/|V_\infty|]$  for the shell drop is less than unity, irrespective of the values of  $K$  and  $M$ . This indicates that the shell drop lags behind the imposed flow. However, the core drop might lag behind or rush ahead of the flow depending on the choice of  $K$  and  $M$ . Indeed, the higher the electric field strength (i.e., higher is the value of  $M$ ), the greater is the intensity of the compound drop to lag behind the flow, as clearly depicted by the slope of the curves for different values of  $M$ . To support this observation, we can recall the distribution of surface charges in Fig. 3, which becomes largely asymmetric with the increase in the value of  $M$ . As a consequence, the charge convection induced retardation also gets enhanced [see the variation of  $U_{i,z}^{(\text{Re}_E)}$  in the insets of Figs. 7(a) and 7(b)]. As a result, the value of longitudinal velocity for a nondeformable compound drop decreases as the Mason number increases. Furthermore, the longitudinal velocity of a nondeformable compound drop decreases as the radius ratio increases. To explain the reason behind such an observation, we can again recall the distribution of surface charges in Fig. 3 which

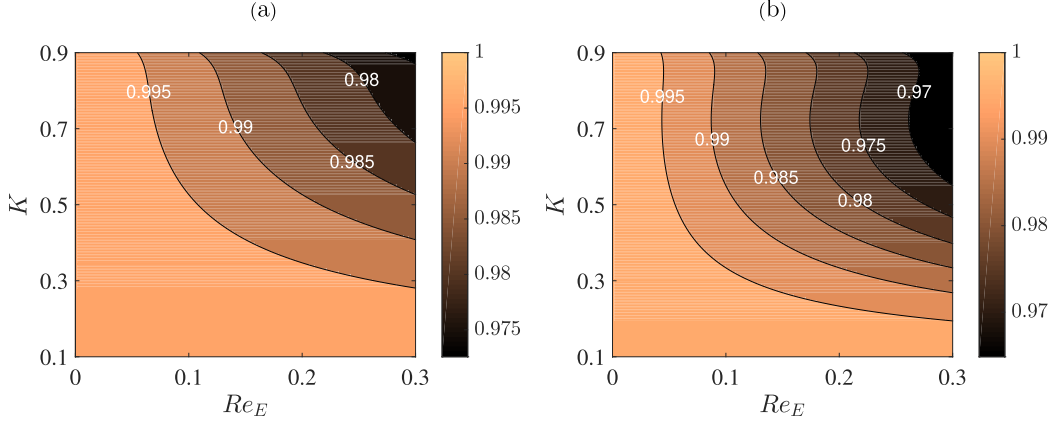


FIG. 8. Mapping of (a)  $\mathfrak{R}_{2,z}^{(Re_E)}$  and (b)  $\mathfrak{R}_{3,z}^{(Re_E)}$  on  $Re_E$ - $K$  plane for  $R_{12} = 0.01$ ,  $R_{13} = 1$ ,  $S_{12} = 0.63$ ,  $S_{13} = 1$ ,  $\lambda_{12} = 0.35$ ,  $\lambda_{13} = 1$ ,  $\theta_t = \pi/4$ ,  $M = 1$ ,  $H = 10$ , and  $x_d = 4$ .

becomes largely asymmetric with the increase in  $K$  and as a consequence, the charge convection induced retardation also gets enhanced. Finally, when the core drop becomes sufficiently small ( $K \leq 0.1$ ), the compound drop arrangement behaves like a single drop and in such a situation, the longitudinal velocity for a nondeformable compound drop becomes independent of  $K$  and minimally influenced by  $M$  [44] and therefore, we observe approximately a constant value when  $K = 0.1$ .

Apart from being a function of  $K$  and  $M$ ,  $U_{i,z}^{(Re_E)}$  is also a function of tilt angle ( $\theta_t$ ) and hence, to depict the critical dependence of an electric field strength and its angle of application, we define an electric field contribution factor as

$$\mathfrak{R}_{i,z}^{(Re_E)} = \frac{U_{i,z}^{(0)} + Re_E U_{i,z}^{(Re_E)}}{(U_{i,z}^{(0)} + Re_E U_{i,z}^{(Re_E)})|_{E_\infty=0}}, \quad i = 2, 3, \quad (98)$$

which quantifies the extent to which the longitudinal drop velocity for a nondeformable drop is altered in the presence of an electric field. The parametric dependence of  $\mathfrak{R}_{i,z}^{(Re_E)}$  with  $i = 2, 3$  on  $\theta_t$  and  $K$  is mapped in Figs. 8(a) and 8(b), respectively. Inspection of these plots reveals that the longitudinal velocity of both the shell and core diminishes as  $K$  increases for all values of  $0 \leq \theta_t \leq \pi/2$ . This result is consistent with the previous discussion. Secondly, we observe that increasing  $\theta_t$  from 0 to  $\pi/2$  increases the longitudinal velocity of both the shell and core of the compound drop. It is observed that changing the direction of the applied electric field has a considerable impact on the antisymmetry in surface charge distribution, and that too significantly on the shell drop. This affects the electrohydrodynamically induced flow and, as a consequence, the resultant interfacial stresses, reducing the drag force on the drop that determines its velocity (Fig. 3).

We also present the effect of  $Re_E$  and  $K$  in modifying the longitudinal drop velocity for a nondeformable compound drop through a map of the parameter,  $\mathfrak{R}_{i,z}^{(Re_E)}$  with  $i = 2, 3$  on the  $\theta_t$ - $K$  plane in Figs. 9(a) and 9(b), respectively. It demonstrates that when the influence of charge convection decreases, the longitudinal velocity of the undeformed shell and core decreases. This happens because the asymmetry in charge distribution is insignificant for lower values of  $Re_E$  (see Fig. 8). Thus, the resultant electrohydrodynamic flow, interfacial stresses, and drag force are minimally influenced, resulting in a lower longitudinal drop velocity. However, as the charge convection effect increases, the electrohydrodynamic flow generates more and more augmentation in the longitudinal velocity for both the shell and core of the drop.

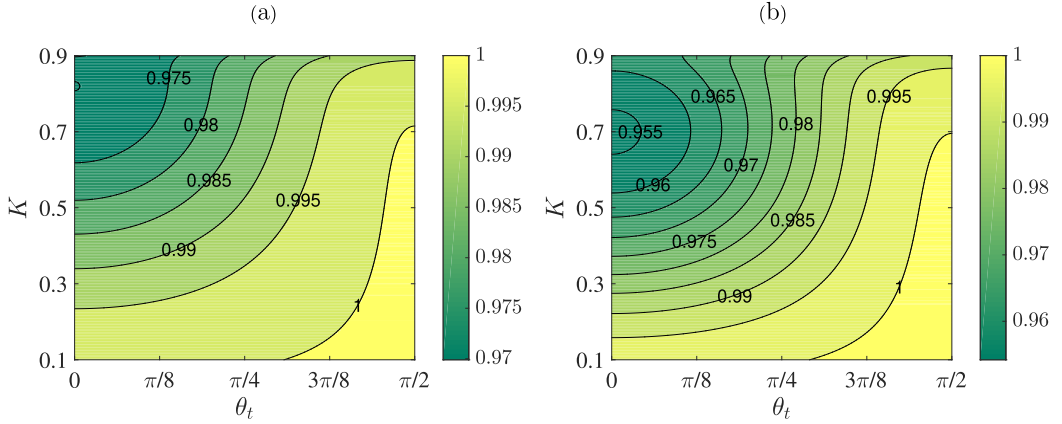


FIG. 9. Mapping of (a)  $\mathfrak{R}_{2,z}^{(Re_E)}$  and (b)  $\mathfrak{R}_{3,z}^{(Re_E)}$  on  $\theta_t$ - $K$  plane for  $R_{12} = 0.01$ ,  $R_{13} = 1$ ,  $S_{12} = 0.63$ ,  $S_{13} = 1$ ,  $\lambda_{12} = 0.35$ ,  $\lambda_{13} = 1$ ,  $Re_E = 0.2$ ,  $M = 1$ ,  $H = 10$ , and  $x_d = 4$ .

## B. Deformable concentric compound drop

### 1. Velocity alteration in the cross-stream direction

The effect of viscosity ratio ( $\lambda_{12}$ ) on the alteration of compound drop velocity in the cross-stream direction is depicted in Fig. 10. The change in viscosity ratio clearly indicates an alteration in the direction of motion for both the shell and core of the drop. Note that the positive and negative values of  $U_{i,x}^{(Ca)}$  indicate the migration of the drop in the positive and negative  $x$  directions, respectively. It can be seen in Fig. 10 that for  $\lambda_{12} \ll 1$ , the shell drop migrates along the negative  $x$  direction, but for  $\lambda_{12} > 1$ , the shell drop moves in the positive  $x$  direction (albeit less as  $U_{2,x}^{(Ca)}$  is close to zero). Similarly, the electric field not only alters the magnitude of  $U_{3,x}^{(Ca)}$  but also the direction of core drop migration, as shown in the inset of Fig. 10. For conditions when the viscosity of the fluid in the shell drop is very much less than the viscosity of the suspending medium, i.e.,  $\lambda_{12} \ll 1$ ,

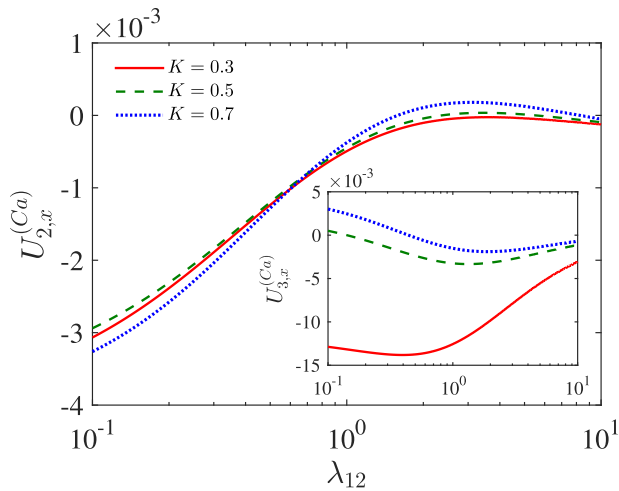


FIG. 10. Variation of lateral velocity due to shape deformation  $U_{2,x}^{(Ca)}$  and  $U_{3,x}^{(Ca)}$  (shown in the inset) with change in  $\lambda_{12}$  for different values of  $K$ . The rest of the parameters are  $R_{12} = 0.01$ ,  $R_{13} = 1$ ,  $S_{12} = 0.63$ ,  $S_{13} = 1$ ,  $\lambda_{13} = 1$ ,  $\theta_t = \pi/4$ ,  $M = 0.1$ ,  $H = 10$ , and  $x_d = 4$ .

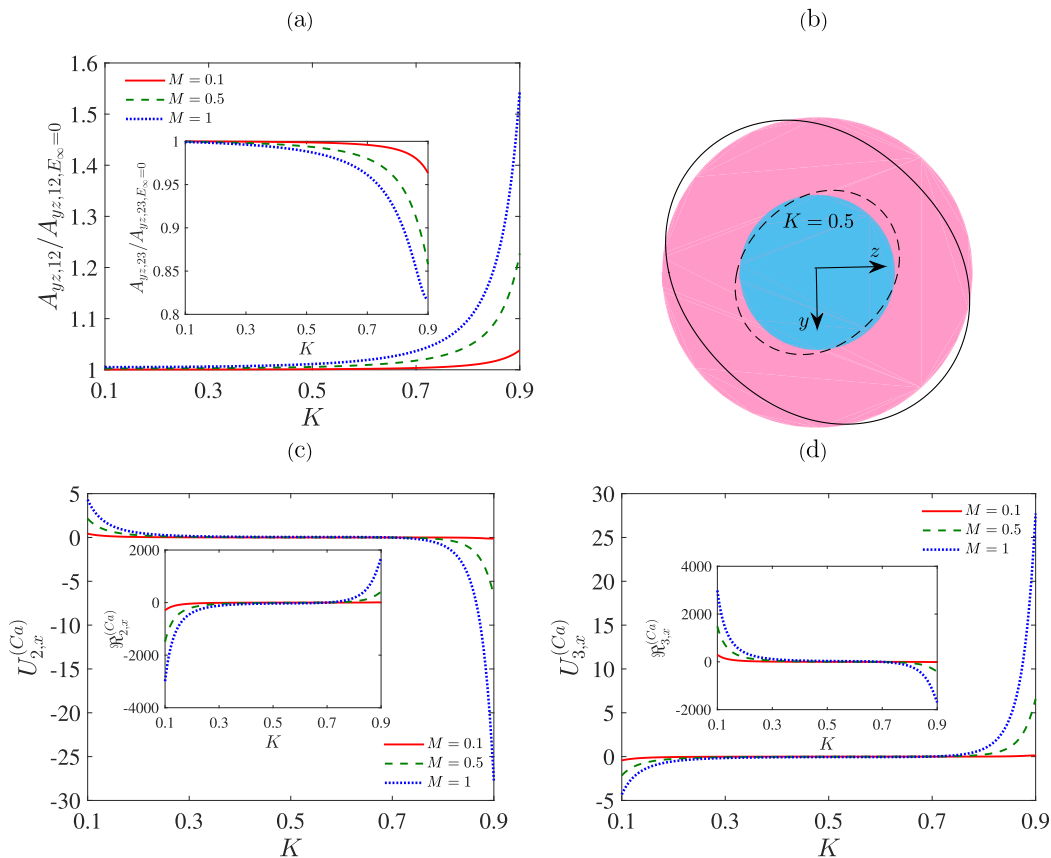


FIG. 11. (a) Variation of drop cross-sectional area perpendicular to the cross-stream direction ( $A_{yz}$ ) for the shell drop (core drop as shown in the inset) with  $K$  for different values of  $M$ . (b) Schematic representation of deformed drop shape (shown by black solid and dashed lines) for the corresponding case when  $K = 0.5$ . (c) Variation of lateral velocity due to shape deformation for the shell drop with  $K$  for different values of  $M$ . (d) Variation of lateral velocity due to shape deformation for the core drop with  $K$  for different values of  $M$ . The inset of panels (c) and (d) depicts the variation of  $\Re_{2,x}^{(Ca)}$  and  $\Re_{3,x}^{(Ca)}$  with  $K$  for different  $M$ . Unless otherwise mentioned, the rest of the parameters are  $R_{12} = 0.01$ ,  $R_{13} = 1$ ,  $S_{12} = 0.63$ ,  $S_{13} = 1$ ,  $\lambda_{12} = 0.35$ ,  $\lambda_{13} = 1$ ,  $\theta_l = \pi/4$ ,  $H = 10$ , and  $x_d = 4$ .

the compound drop arrangement resembles the behavior of a bubble encompassing a drop. As a result, the deformation is maximum for both the shell and core drops and hence the magnitude of cross-stream velocity is also higher for  $\lambda_{12} \ll 1$ . However, for  $\lambda_{12} \gg 1$ , the dynamics of the shell drop resembles that of a solid sphere, resulting in less deformation and rendering the compound drop practically immobile.

Toward explaining the effect of drop deformation on the alteration of velocity for both the shell and core drops in the cross-stream direction, we look into the variation of the cross-section of the drop perpendicular to the lateral direction ( $A_{yz}$ ). In Fig. 11(a), we present the variation of  $A_{yz}$  for both the shell and the core drops due to change in  $K$  and  $M$ . It can be seen that, as the radius ratio increases, the cross-section of the shell drop perpendicular to the lateral direction increases, while the cross-section of the core drop decreases. Such a variation is supported by the deviation of compound drop shape from sphericity as shown in Fig. 11(b). Although the drop shape is dependent on the combination of  $R_{12}$  and  $S_{12}$ , the considered values of electrical property ratios for Fig. 11(b) produces oblate and prolate deformation patterns (with respect to the direction of the



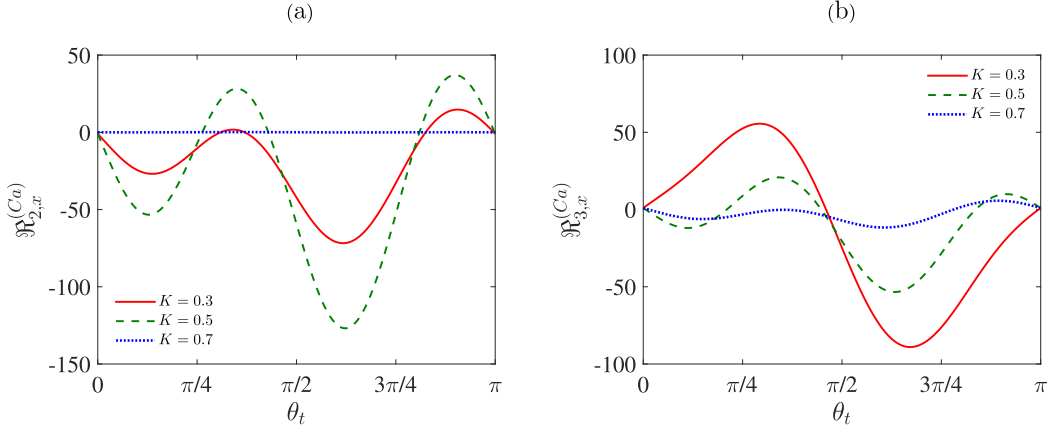


FIG. 12. Variation of  $\mathfrak{R}_{2,x}^{(Ca)}$  and  $\mathfrak{R}_{3,x}^{(Ca)}$  with  $\theta_t$  for different  $K$ . The rest of the parameters are  $R_{12} = 0.01$ ,  $R_{13} = 1$ ,  $S_{12} = 0.63$ ,  $S_{13} = 1$ ,  $\lambda_{12} = 0.35$ ,  $\lambda_{13} = 1$ ,  $M = 0.5$ ,  $H = 10$ , and  $x_d = 4$ .

applied electric field) for the shell and core drops, respectively; this follows the theory proposed by Taylor [1]. It has been observed that application of the electric field increases the cross-section of the shell drop that undergoes oblate deformation while decreases the cross-section of the core drop that undergoes prolate deformation. Moreover, the higher the radius ratio of the compound drop, the lesser is the annular space, and therefore the stronger the electrohydrodynamically induced flow and interfacial stresses. As a consequence, the effect of the electric field on the alteration of drop cross-section increases substantially as the value of  $K$  increases. For higher values of  $M$ , the effect of the electric field is much more pronounced, resulting in a greater alteration in the drop cross-section perpendicular to the cross-stream direction.

The alteration of drop cross-section accordingly changes the flow resistance and this, in turn, dictates the cross-stream velocity of the compound drop. The cross-stream velocities of the shell and core drops due to change in  $K$  and  $M$  are presented in Figs. 11(c) and 11(d), respectively. In tune with the variation of the drop's cross-section perpendicular to the cross-stream direction, the cross-stream velocity of the drop also augments quantitatively with the increase in  $K$  and  $M$ . Interestingly, even for lower values of the radius ratio, the cross-stream velocity of the compound drop increases in magnitude due to the decrement in  $K$  and increment in  $M$ . This can be attributed to the amplified effect of the applied electric field on the cross-stream velocity when the radius ratio is either very low or very high. For this, we define another electric field contribution factor as

$$\mathfrak{R}_{i,x}^{(Ca)} = \frac{U_{i,x}^{(Ca)}}{(U_{i,x}^{(Ca)})|_{E_\infty=0}}, \quad i = 2, 3, \quad (99)$$

and we present their variation with  $K$  and  $M$  in the insets of Figs. 11(c) and 11(d), respectively. Furthermore, it can be observed that, at lower radius ratio, the shell drop accelerates, while it exhibits retardation when the radius ratio is high. On the contrary, the opposite is true for the core drop.

Figure 12 depicts the variation of  $\mathfrak{R}_{i,x}^{(Ca)}$  with  $\theta_t$  and  $K$  for a compound drop initially placed at an off-center location. The values of the rest of the parameters are provided in the figure caption. It can be observed that the effect of tilt angle of the applied electric field in accelerating or retarding the motion of compound drop gets dampened out or minimized when the size of the core drop increases (i.e., as the value of  $K$  is increased). When the applied electric field is axial ( $\theta_t = 0$  or  $\pi$ ), the Mason number has no effect in altering the compound drop velocity. It is also observed that, unlike the case of a single drop where the effect of the Mason number in altering the deformation triggered cross-stream velocity gets nullified for  $\theta_t = 0$  and  $\pi/2$ . This happens because when an electric field is applied to a compound drop at an angle other than the imposed flow direction (positive

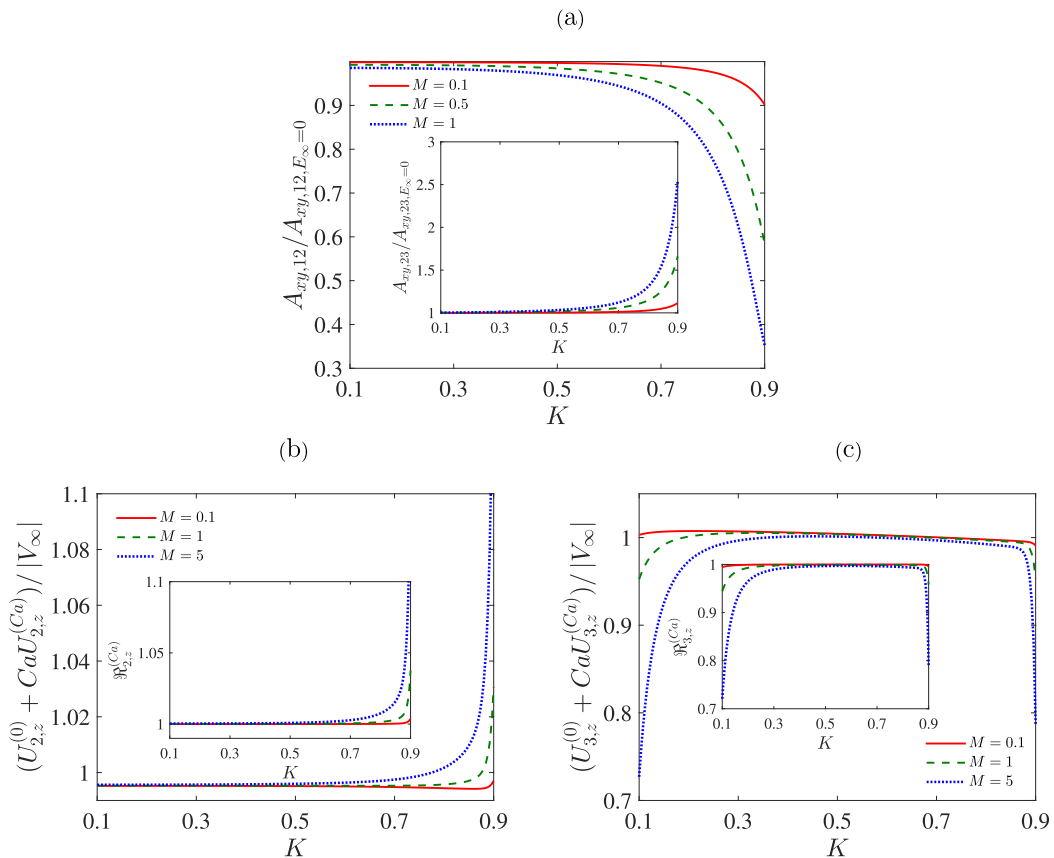


FIG. 13. (a) Variation of relative projected area of the drop in the  $x$ - $y$  plane ( $A_{xy,12}/A_{xy,12,E_\infty=0}$ ) for the shell drop with  $K$  for different values of  $M$ ; the inset of this panel shows the variation of ( $A_{xy,23}/A_{xy,23,E_\infty=0}$ ) with  $K$  for the core drop. (b) Variation of  $(U_{2,z}^{(0)} + CaU_{2,z}^{(Ca)})/|V_\infty|$  with  $K$  for different values of  $M$ ; the inset shows the variation of  $\mathfrak{R}_{2,z}^{(Ca)}$  with  $K$ . (c) Variation of  $(U_{3,z}^{(0)} + CaU_{3,z}^{(Ca)})/|V_\infty|$  with  $K$  for different values of  $M$ ; the inset shows the variation of  $\mathfrak{R}_{3,z}^{(Ca)}$  with  $K$ . Unless otherwise mentioned, the rest of the parameters are  $R_{12} = 0.01$ ,  $R_{13} = 1$ ,  $S_{12} = 0.63$ ,  $S_{13} = 1$ ,  $\lambda_{12} = 0.35$ ,  $\lambda_{13} = 1$ ,  $\theta_t = \pi/4$ ,  $Ca = 0.1$ ,  $H = 10$ , and  $x_d = 4$ .

or negative), the deformation-triggered cross-stream velocity is altered not only by hydrodynamic effects, but also by the effects of the applied electric field.

## 2. Velocity alteration in the longitudinal direction

Next, we explore the alteration of deformed compound drop velocity in the longitudinal direction. Before that, we analyze the possible variation of the drop cross-section perpendicular to the longitudinal direction ( $A_{xy}$ ) in Fig. 13(a) where we present the variation of  $A_{xy}$  for both the shell and core drops due to change in  $K$  and  $M$ . It can be seen that as the radius ratio increases, the cross-section of the shell drop perpendicular to the longitudinal direction exponentially decreases, while the cross-section of the core drop exponentially increases. Furthermore, as in the previous case, the effect of the electric field on the alteration in drop cross-section increases dramatically as the value of  $K$  increases. Furthermore, when the value of  $M$  increases, the effect of the electric field becomes more pronounced, resulting in a bigger change in the drop cross-section perpendicular to the cross-stream direction.

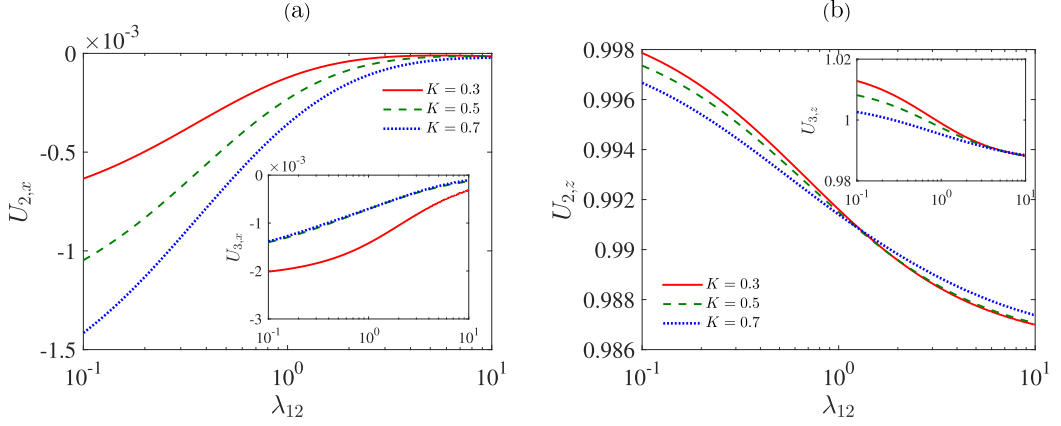


FIG. 14. Variations of (a) the lateral velocity due to the combined effect of charge convection and shape deformation  $U_{2,x}$  ( $U_{3,x}$  as shown in the inset), and (b) the longitudinal velocity due to the combined effect of charge convection and shape deformation  $U_{2,z}$  ( $U_{3,z}$  as shown in the inset) with change in  $\lambda_{12}$  for different values of  $K$ . The rest of the parameters are  $R_{12} = 0.01$ ,  $R_{13} = 1$ ,  $S_{12} = 0.63$ ,  $S_{13} = 1$ ,  $\lambda_{13} = 1$ ,  $\theta_t = \pi/4$ ,  $M = 0.1$ ,  $\text{Re}_E = 0.1$ ,  $\text{Ca} = 0.1$ ,  $H = 10$ , and  $x_d = 4$ .

The alteration of drop cross-section accordingly affects the flow resistance and this, in turn, dictates the longitudinal velocity of the compound drop. It is important to note that the longitudinal velocity of a deformed compound drop is the combined effects of leading-order velocity and deformation-induced velocity. In Figs. 13(b) and 13(c), we present the longitudinal velocity of the shell and core drops due to change in  $K$  and  $M$ , respectively. As the radius ratio of the compound drop increases, the shell drop tries to rush ahead of the imposed flow. To explain the reason behind such a variation, we define another electric field contribution factor as

$$\mathfrak{R}_{i,z}^{(\text{Ca})} = \frac{U_{i,z}^{(0)} + \text{Ca}U_{i,z}^{(\text{Ca})}}{(U_{i,z}^{(0)} + \text{Ca}U_{i,z}^{(\text{Ca})})|_{E_\infty=0}}, \quad i = 2, 3. \quad (100)$$

The variation of  $\mathfrak{R}_{2,z}^{(\text{Ca})}$  indicates that the effect of an electric field on the longitudinal velocity gets amplified when the radius ratio increases. This, in turn, changes the area of the deformed drop shape, the drag force, and hence, the longitudinal velocity of the shell drop. However, it is found that the core drop lags behind the imposed flow when the radius ratio is either very low or very high. Although, the area of the core drop only increases at a higher radius ratio, however, it is found from the variation of  $\mathfrak{R}_{3,z}^{(\text{Ca})}$  that the effect of the electric field in altering the longitudinal velocity of the core drop is predominant when the radius ratio is either very low or very high. In particular, the retardation observed at lower radius ratios is primarily due to the effect of the applied electric field in altering the leading-order velocity, while at higher values of  $K$ , the change in the longitudinal velocity of the core drop is the result of the deformation-induced change in the drag force. Furthermore, the deformation pattern (prolate deformation for shell drop and oblate deformation for core drop) is the reason behind the fact that the longitudinal velocity of the shell drop is higher than the imposed flow, while that of the core drop is generally lower than the imposed flow velocity. Also, as the value of  $M$  increases, the affinity of the shell drop to rush ahead and the core drop to lag behind the imposed flow increases.

### C. Combined effect of charge convection and shape deformation

In Fig. 14, we present the influence of viscosity ratio ( $\lambda_{12}$ ) on the alteration of cross-stream velocity and longitudinal velocity of the shell and core drops due to the combined effect of charge

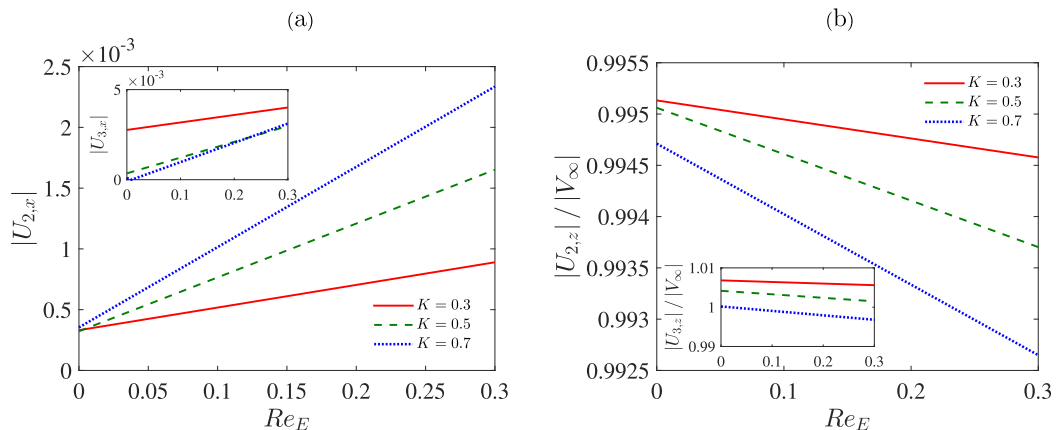


FIG. 15. Variations of (a)  $|U_{2,x}|$  ( $|U_{3,x}|$  as shown in the inset), and (b)  $|U_{2,z}|/|V_\infty|$  ( $|U_{3,z}|/|V_\infty|$  as shown in the inset) with change in  $Re_E$  for different values of  $K$ . The rest of the parameters are  $R_{12} = 0.01$ ,  $R_{13} = 1$ ,  $S_{12} = 0.63$ ,  $S_{13} = 1$ ,  $\lambda_{12} = 0.35$ ,  $\lambda_{13} = 1$ ,  $\theta_t = \pi/4$ ,  $M = 0.1$ ,  $Ca = 0.1$ ,  $H = 10$ , and  $x_d = 4$ .

convection and shape deformation and for various radius ratio of the compound drop. It is found that for  $\lambda_{12} \ll 1$ , the magnitude of the lateral velocity of both the shell and core drops is very high because in this case, the compound drop arrangement behaves like a bubble. However, for  $\lambda_{12} \gg 1$ , the compound drop arrangement behaves like a rigid sphere, and therefore, the effects of charge convection and shape deformation are decreased, thus resulting in low magnitude of the cross-stream velocity. Also, as the radius ratio increases, the magnitude of the cross-stream velocity of the shell drop increases, while the cross-stream velocity of the core drop decreases. Moreover, in the presence of charge convection, the alteration in the direction of lateral migration observed due to the influence of shape deformation as illustrated in Fig. 10 is not apparent. This is because the direction of lateral migration is dictated by the competition between the influence of charge convection and shape deformation. In terms of the longitudinal velocity alteration, it can be seen from Fig. 14 that the velocity decreases with the increase in the viscosity ratio. Additionally, the longitudinal velocity is higher for lower values of  $K$  when  $\lambda_{12} \ll 1$ , but beyond a certain critical value of  $\lambda_{12}$ , the longitudinal velocity is higher for higher values of  $K$  for both the shell and core drops.

Figure 15 depicts the variation in the magnitude of lateral and longitudinal velocity for both the shell and core of the drop with different radius ratios due to change in  $Re_E$  when the combined effects of charge convection and shape deformation are taken into account. The rest of the parameters are provided in the figure caption. Considering a fixed  $Ca$ , it is seen that an increase in  $Re_E$  enhances the lateral velocity of both the shell and core drops, while the longitudinal velocity is decreased. Such a variation is related to the orientation of charge distribution on the surface of the shell and core drops as previously shown in Figs. 3 and 4. It is found that the lateral velocity of the shell drop increases with the increase in  $K$ , while that of the core drop decreases with the increase in  $K$ . However, the longitudinal velocity of both the shell and core drops decreases with the increase in  $K$ . Furthermore, at lower values of  $Re_E$ , the longitudinal velocity of the core drop is higher than the free stream velocity, while depending on the value of  $K$ , the longitudinal velocity might be lower than the free stream velocity beyond a certain value of  $Re_E$ . Similarly, considering a fixed value of  $Re_E$ , when we vary  $Ca$ , then it can be observed in Fig. 16 that the magnitude of the lateral and longitudinal velocity of the shell and core drops increases with an increase in  $Ca$  due to greater deformation.

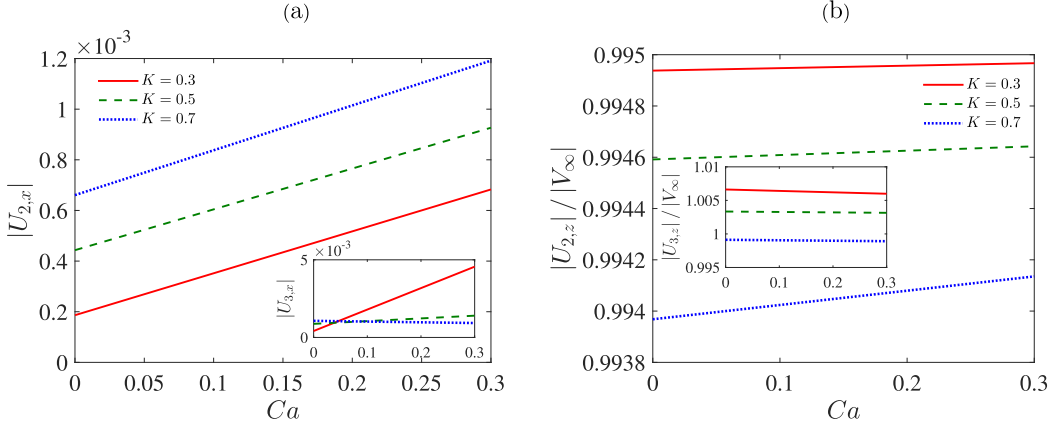


FIG. 16. Variations of (a)  $|U_{2,x}|$  ( $|U_{3,x}|$  as shown in the inset) and (b)  $|U_{2,z}|/|V_\infty|$  ( $|U_{3,z}|/|V_\infty|$  as shown in the inset) with change in  $Ca$  for different values of  $K$ . The rest of parameters are  $R_{12} = 0.01$ ,  $R_{13} = 1$ ,  $S_{12} = 0.63$ ,  $S_{13} = 1$ ,  $\lambda_{12} = 0.35$ ,  $\lambda_{13} = 1$ ,  $\theta_t = \pi/4$ ,  $M = 0.1$ ,  $Re_E = 0.1$ ,  $H = 10$ , and  $x_d = 4$ .

Under the quasisteady-state approximation, we also determine the quasisteady-state droplet trajectory by solving the following differential equations

$$\frac{dx_d(t)}{dt} = Re_E U_{i,x}^{(Re_E)} + Ca U_{i,x}^{(Ca)}, \quad (101)$$

$$\frac{dz_d(t)}{dt} = U_{i,z}^{(0)} + Re_E U_{i,z}^{(Re_E)} + Ca U_{i,z}^{(Ca)}, \quad (102)$$

where,  $x_d$  and  $z_d$  represents the nondimensional transverse and axial position of the compound drop centroid. With a suitable choice of the initial position of the compound drop, we can solve the above equations using appropriate numerical techniques. The quasisteady-state trajectory of the shell and core drop is plotted in Fig. 17 for different values of radius ratio and two different combinations of conductivity and permittivity ratios, considering the initial centroid of the compound drop to be located at an off-centre location, i.e.,  $x_d = 4$ . The rest of the parameters are provided in the

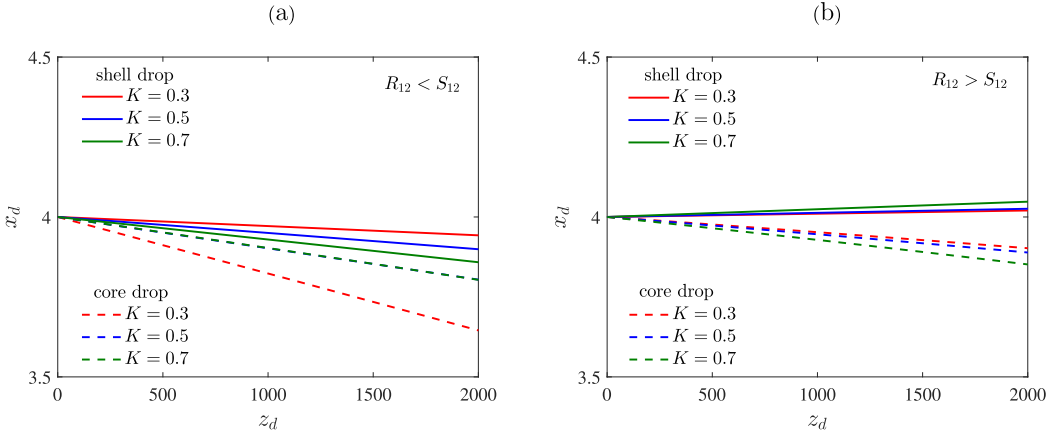


FIG. 17. Trajectory of the shell and core drop for different radius ratio and for (a)  $R_{12} = 0.01$ ,  $S_{12} = 0.63$ , and (b)  $R_{12} = 2$ ,  $S_{12} = 0.5$  using the concentric compound drop theory. The rest of the parameters are  $R_{13} = 1$ ,  $S_{13} = 1$ ,  $\lambda_{12} = 0.35$ ,  $\lambda_{13} = 1$ ,  $\theta_t = \pi/4$ ,  $M = 0.1$ ,  $Re_E = 0.01$ ,  $Ca = 0.01$ ,  $H = 10$ , and  $x_d(t = 0) = 4$ .

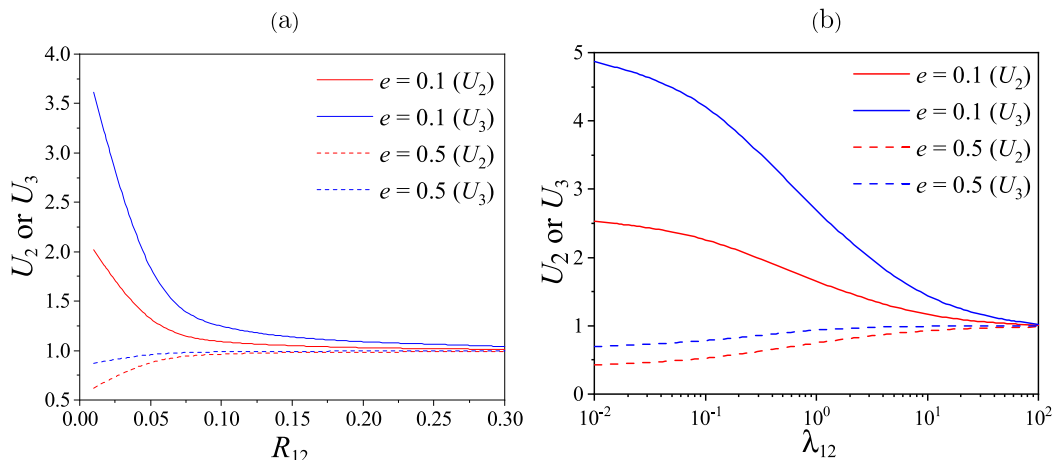


FIG. 18. (a) Variation of shell and core drop velocity with  $R_{12}$  for different value of eccentricity of the compound drop. The rest of the parameters are  $R_{13} = 1$ ,  $S_{12} = 0.63$ ,  $S_{13} = 1$ ,  $\lambda_{12} = 0.35$ ,  $\lambda_{13} = 1$ ,  $H = 10$ , and  $K = 0.2$ . (b) Variation of shell and core drop velocity with  $\lambda_{12}$  for different value of eccentricity of the compound drop. The rest of the parameters are  $R_{12} = 0.01$ ,  $R_{13} = 1$ ,  $S_{12} = 0.63$ ,  $S_{13} = 1$ ,  $\lambda_{13} = 1$ ,  $H = 10$ , and  $K = 0.2$ .

figure caption. Previously Mortazavi and Tryggvason [62] have shown that a single drop under plane Poiseuille flow can either migrate toward the channel centreline or toward the wall depending on the hydrodynamic properties. In the present study, we find that for  $R_{12} < S_{12}$ , both the shell and core drop migrate toward the channel wall, irrespective of the radius ratio. However, the core drop traverses a greater distance toward the wall, resulting in very minimal eccentricity and within the limit of valid concentric assumption. On the contrary, when  $R_{12} > S_{12}$ , it is seen that the shell drop migrates toward the channel centreline, while the core drop migrates toward the wall due to asymmetric charge distribution and fluid circulation.

#### D. Eccentric compound drop under plane Poiseuille flow and an electric field

We have also briefly presented the results for the specific example of the axisymmetric motion of eccentric compound drop under the action of background plane Poiseuille flow and subjected to an externally imposed electric field applied along the flow direction as shown in the schematic Fig. 2. We begin our discussion by presenting the variation of shell and core drop velocities with conductivity ratio ( $R_{12}$ ) for two different values of eccentricity in Fig. 18(a). We find that depending on the eccentricity value, the velocity of shell and core drop increases or decreases with the increase in conductivity ratio. For lower eccentricity values, we observe a decrease in shell and core drop velocity with the increase in conductivity ratio, while the reverse is the case for higher ones of eccentricity. This happens because of the imbalance of fluid accumulation upstream and downstream of the core drop due to the change in eccentricity. Moreover, we also find that the effect of eccentricity on the velocity of the compound drop is nullified when the conductivity ratio is significantly higher. This can be attributed to the decrement in asymmetric charge distribution with the increase in conductivity ratio. We have also presented the variation of shell and core drop velocities with viscosity ratio for different eccentricity values in Fig. 18(b). The rest of the parameters are provided in the figure caption. Here also, we observe that depending on the value of eccentricity, the velocity of shell and core drop either increases or decreases with the increase in viscosity ratio due to the asymmetry in fluid accumulated upstream and downstream of the core drop. Moreover, we also observe significant variation in velocity at lower values of viscosity ratio, while at sufficiently higher viscosity ratio, the velocities tend to a finite value.



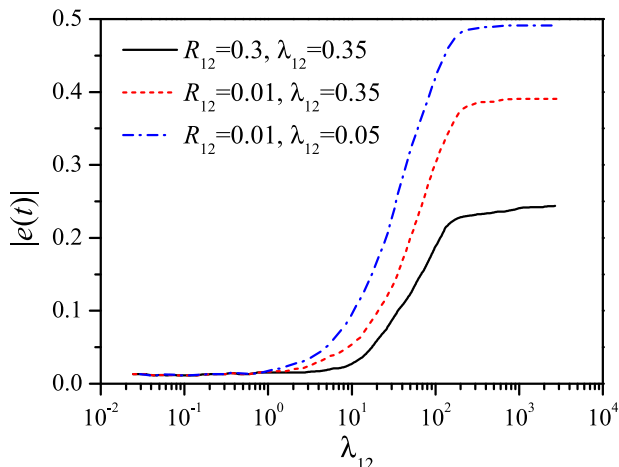


FIG. 19. Variation of eccentricity with nondimensional time for different combinations of  $R_{12}$  and  $\lambda_{12}$  using the eccentric compound drop theory. The rest of the parameters are  $R_{13} = 1$ ,  $S_{13} = 1$ ,  $\lambda_{13} = 1$ ,  $H = 10$ , and  $K = 0.2$ .

Since the shell and core drop do not move with the same velocities hence, the eccentricity would change with time. Considering the implicit time dependence, we determine the evolution of eccentricity with time by numerically solving the following differential equation:

$$\frac{de}{dt} = \{U_3[e(t), \Pi] - U_2[e(t), \Pi]\}. \quad (103)$$

Based on the solution of Eq. (103), we have plotted the temporal variation of eccentricity for different combination of conductivity ratio and viscosity ratio in Fig. 19 subjected to an initial concentric configuration. From the evolution of eccentricity, it is clear that the concentric compound drop maintains its stable position upto a certain time beyond which the eccentricity starts to increase. This critical time of transition from stable to unstable position differs with the change in concomitant electrical and hydrodynamic parameters. Furthermore, at a sufficiently longer time, the equilibrium position is attained and the value of eccentricity becomes stagnant. Further details on the limit of eccentricity and the critical time limit for the concentric assumption to remain valid is discussed in Appendices A and H.

#### IV. CONCLUSIONS

The dynamics of a concentric compound drop migrating and deforming in a plane Poiseuille flow under the influence of an arbitrarily orientated uniform electric field is investigated analytically using regular perturbation theory. A double asymptotic approach is employed with the electric Reynolds number ( $Re_E$ ) and the capillary number ( $Ca$ ) as small perturbation parameters to account for the effects of charge convection and shape deformation and the governing equations for surface charge distribution, deformed interface shape, and migration velocity of the shell and core drops are derived. Under the single drop limit, the expressions of velocity and deformed interface obtained using the current model agree with the combined analytical and experimental investigation of Taylor [1] and the analytical study of Chan and Leal [48]. The underlying physics is thoroughly studied by altering the hydrodynamic ( $\lambda_{12}$ ), electrical ( $R_{12}$ ,  $S_{12}$ ,  $\theta_t$ ), and physical ( $K$ ) parameters for the compound drop.

We found that when the tilt angle of the applied electric field is  $\pi/4$ , the disturbance in the antisymmetric distribution of charges on the surface of the shell drop is maximum. However, in terms of the magnitude of positive and negative charges, the antisymmetry in the distribution of

charges on the surface of the core drop is disrupted. The antisymmetric charge distribution on the surface of the shell and core drops increases with the increase in the Mason number, electric Reynolds number, and radius ratio of the compound drop. The magnitude of charges on the surface of the core drop increases as the radius ratio of the compound drop increases. Moreover, it is observed that the polarity of the charges on the surfaces of the shell drop is opposite to that on the surface of the core drop. In the case of a nondeformable compound drop, the maximum retardation due to charge convection for both the shell and core drop occurs when the viscosity of shell drop is much less than that of the suspending medium, i.e.,  $\lambda_{12} \ll 1$ ; the reverse happens for  $\lambda_{12} \gg 1$ . We found that the magnitude of the lateral velocity (longitudinal velocity) due to charge convection for both the shell and core drops increases (decreases) with the increase in radius ratio; the longitudinal velocity of both the shell and core drops diminishes with increasing  $K$  for all values of  $0 \leq \theta_t \leq \pi/2$ . It is observed that increasing the electric field strength (i.e., increasing  $M$ ) increases the lagging tendency of the shell drop behind the imposed flow.

In the case of a deformable compound drop without charge convection, it is found that the shell drop migrates along the negative and positive  $x$  direction for  $\lambda_{12} \ll 1$  and  $\lambda_{12} > 1$ , respectively. For low radius ratios, the magnitude of the cross-stream velocity increases as  $K$  decreases and  $M$  increases. The shell drop accelerates when the radius ratio is low and decelerates when the radius ratio is high. The dynamics of the core drop, on the other hand, is exactly the reverse. When the size of the core drop gets bigger, the effect of the tilt angle of the electric field on changing the direction of motion of deformable compound drops is dampened. While the effect of the electric field on longitudinal velocity increases as the radius ratio increases, its effect in altering the longitudinal velocity of the core drop is predominant when the radius ratio is either extremely low or high. Furthermore, when the value of  $M$  increases, the affinity of the deformable shell drop to rush ahead, and the core drop to lag behind the imposed flow increases.

Under the combined action of charge convection and shape deformation, the longitudinal velocity is higher for lower values of  $K$  for  $\lambda_{12} \ll 1$ , but beyond a certain critical value of  $\lambda_{12}$ , the longitudinal velocity is higher for higher values of  $K$  for both the shell and core drops. For a fixed  $Ca$ , it is seen that increasing  $Re_E$  enhances the lateral velocity and decreases the longitudinal velocity of both the shell and core drops. However, for a fixed value of  $Re_E$ , it is found that the magnitude of lateral and longitudinal velocities of the shell and core drops increases with an increase in  $Ca$ . Moreover, by determining the quasisteady-state compound droplet trajectory, we found that the shell and core drop can either migrate along the same direction (i.e., toward the channel centreline or toward the wall) or opposite direction depending on the combination of electrical conductivity and permittivity ratios.

Finally, by solving for the velocity field of an eccentric compound drop under plane Poiseuille flow and subjected to an applied electric field, we found that the concentric and eccentric compound drop configurations show similar results up to an eccentricity value of less than 0.1 and a dimensionless time interval of the order of 10.

#### ACKNOWLEDGMENTS

K.C.S. thanks Science and Engineering Research Board, India for providing financial support (Grant No. CRG/2020/000507). The authors are also very grateful to Sayali N. Jadhav and Uddipta Ghosh of the Department of Mechanical Engineering, Indian Institute of Technology Gandhinagar for insightful discussions related to the eccentric compound drop theory.

#### APPENDIX A: JUSTIFICATION OF THE ASSUMPTIONS

To justify the parametric space used in our simulations, let us consider the core drop and the suspending medium to be castor oil ( $\rho_{1,3} = 960 \text{ Kg/m}^3$ ,  $\mu_{1,3} = 1.4 \text{ Pa s}$ ,  $\epsilon_{1,3} = 4.45\epsilon_0$ ,  $\sigma_{1,3} = 10^{-10} \text{ S/m}$ ) with  $\epsilon_0$  being the permittivity of free space, and the fluid in the shell drop to be phenylmethylsiloxane-dimethylsiloxane (PMM) ( $\rho_2 = 960 \text{ Kg/m}^3$ ,  $\mu_2 = 0.5 \text{ Pa s}$ ,  $\epsilon_2 = 2.8\epsilon_0$ ,

$\sigma_2 = 10^{-12}$  S/m) having a surface tension  $\gamma = 5 \times 10^{-3}$  N/m, as previously considered in the experiments of Xu and Homsy [45]. Considering a compound drop with an outer radius of 3 mm and subjected to an electric field strength of  $5 \times 10^5$  V/m and background Poiseuille flow of centerline velocity  $V_c = 1$  mm/s will justify the assumptions considered in the present study in the following way. These fluids are assumed to be Newtonian and immiscible. Considering these properties, the charge relaxation timescale,  $\varepsilon_1/\sigma_1$ , is less than the convective timescale,  $R_o/U_c$ , rendering the validity of the leaky dielectric theory. The aforementioned property values will result in  $\text{Re} \sim 10^{-3}$ , allowing us to assume the Stokes flow. For this set of parameters, the capillary number,  $\text{Ca} \sim 0.1$ . Thus, the deviation of the drop interface shape from sphericity can be neglected. Moreover, it is intuitive that the droplets would move, which would naturally lead to the temporal evolution of the whole compound drop configuration. Therefore, we have assumed the flow to be quasisteady, enabling us to neglect the temporal derivative on the left-hand side of the Navier–Stokes equations. As a result, the fluid motion at a given time becomes a function of the instantaneous location of the droplet. It should also be noted that the assumption of quasisteady flow while studying the creeping motion of droplets is abundant in the literature [44,63,64]. Also, the aforementioned property values will result in an electric Reynolds number ( $\text{Re}_E = \varepsilon_1 V_c / R_o \sigma_1$ ) of the order of 0.1 and Saville number ( $\text{Sa} = \text{Re}_E / \text{Ca}_E$ ) of the order of 0.005. As  $\text{Sa} \ll \text{Re}_E$ , our assumptions of keeping the charge convection term and dropping the current term are also justified.

Regarding the assumption of stable compound drop, experiments performed by Ficheux *et al.* [65], Utada *et al.* [66], Pal [67], Kim *et al.* [68] on the generation of double emulsions have shown that using novel techniques, such as actuating biphasic flow in narrow capillaries [68], one can generate stable double emulsions, even when the shell-drop thickness is minimal (submicron range). Moreover, the methods employed in these studies have further offered a high degree of control over droplet sizes. With the aforementioned experimental stand, it is thus justified and practically feasible to consider a stable compound drop configuration for our study. Lastly, the assumption of concentric compound drop configuration while studying the creeping motion of a droplet has been considered in the literature [25,30,31,35,38,43]. Practically, it has been shown by Bei *et al.* [69–71] through laboratory experiments that the application of an electric field can produce a highly concentric foam shell with ease. Bei *et al.* [69,70], Tucker-Schwartz *et al.* [72] observed that it is possible to create a highly concentric compound drop at any value of the core dielectric constant in an electric field. Later, Bei *et al.* [71] found that the quality of a concentric compound drop can be improved when the strength of the applied electric field is high enough to overcome the electrostatic shielding. Hence, having the scope of generating concentric compound drops through experimental strategies, we have found it practically valid to assume compound drops to be concentric for our analytical study.

Moreover, to confirm the validity of the assumption of compound drop to be concentric, we define the relative velocity between the two drops as  $W = |(U_{2,z} - U_{3,z})/U_{2,z}|$ . It is quite clear that, in general, the shell and the core drop might move with different velocities and therefore, for the concentric drop approximation to remain valid, one must have  $e \ll 1$ ,  $e$  being the eccentricity. However, the eccentricity in the compound drop system would still increase at a linear rate as follows:  $e(t) = (U_{2,z} - U_{3,z})t = WU_{2,z}t$ . From this expression, it is quite clear that, even with  $W \ll 1$  and  $U_{2,z} \sim O(1)$ , the eccentricity would become large for  $t \sim O(W^{-1})$ . This leads to the conclusion that the concentric theory can be expected to furnish approximately correct results only for low values of eccentricity ( $e$ ), or, in other words, for  $t < W^{-1}$ .

## APPENDIX B: EXPRESSIONS FOR THE GROWING AND DECAYING SOLID HARMONICS IN Eqs. (46)–(51)

The growing solid harmonics  $p_n^{(k)(i)}$ ,  $\phi_n^{(k)(i)}$ , and  $\chi_n^{(k)(i)}$  can be expressed as

$$p_n^{(k)(i)} = \lambda_{1i} r^n \sum_{m=0}^n [A_{n,m}^{(k)(i)} \cos(m\phi) + \hat{A}_{n,m}^{(k)(i)} \sin(m\phi)] P_{n,m}(\cos\theta), \quad (\text{B1})$$

$$\phi_n^{(k)(i)} = r^n \sum_{m=0}^n [B_{n,m}^{(k)(i)} \cos(m\phi) + \hat{B}_{n,m}^{(k)(i)} \sin(m\phi)] P_{n,m}(\cos\theta), \quad (\text{B2})$$

$$\chi_n^{(k)(i)} = r^n \sum_{m=0}^n [C_{n,m}^{(k)(i)} \cos(m\phi) + \hat{C}_{n,m}^{(k)(i)} \sin(m\phi)] P_{n,m}(\cos\theta). \quad (\text{B3})$$

The decaying solid harmonics  $p_{-n-1}^{(k)(i)}$ ,  $\phi_{-n-1}^{(k)(i)}$ , and  $\chi_{-n-1}^{(k)(i)}$  are given by

$$p_{-n-1}^{(k)(i)} = \lambda_{1i} r^{-n-1} \sum_{m=0}^n [A_{-n-1,m}^{(k)(i)} \cos(m\phi) + \hat{A}_{-n-1,m}^{(k)(i)} \sin(m\phi)] P_{n,m}(\cos\theta), \quad (\text{B4})$$

$$\phi_{-n-1}^{(k)(i)} = r^{-n-1} \sum_{m=0}^n [B_{-n-1,m}^{(k)(i)} \cos(m\phi) + \hat{B}_{-n-1,m}^{(k)(i)} \sin(m\phi)] P_{n,m}(\cos\theta), \quad (\text{B5})$$

$$\chi_{-n-1}^{(k)(i)} = r^{-n-1} \sum_{m=0}^n [C_{-n-1,m}^{(k)(i)} \cos(m\phi) + \hat{C}_{-n-1,m}^{(k)(i)} \sin(m\phi)] P_{n,m}(\cos\theta), \quad (\text{B6})$$

where  $A_{n,m}^{(k)(i)}$ ,  $\hat{A}_{n,m}^{(k)(i)}$ ,  $A_{-n-1,m}^{(k)(i)}$ ,  $\hat{A}_{-n-1,m}^{(k)(i)}$ ,  $B_{n,m}^{(k)(i)}$ ,  $\hat{B}_{n,m}^{(k)(i)}$ ,  $B_{-n-1,m}^{(k)(i)}$ ,  $\hat{B}_{-n-1,m}^{(k)(i)}$ ,  $C_{n,m}^{(k)(i)}$ ,  $\hat{C}_{n,m}^{(k)(i)}$ ,  $C_{-n-1,m}^{(k)(i)}$  and  $\hat{C}_{-n-1,m}^{(k)(i)}$  are the unknown coefficients.

### APPENDIX C: EXPRESSIONS FOR THE LEADING-ORDER VELOCITY AND PRESSURE DISTRIBUTIONS WITHIN THE CORE AND SHELL REGIONS AND OUTSIDE THE COMPOUND DROP IN TERMS OF SPHERICAL HARMONICS

$$\begin{aligned} \mathbf{u}_1^{(0)} &= \nabla \times (\mathbf{r}\chi_{-3}^{(0)(1)}) + \nabla(\phi_{-4}^{(0)(1)} + \phi_{-3}^{(0)(1)} + \phi_{-2}^{(0)(1)}) \\ &\quad + r^2 \left( \frac{1}{2} \nabla p_{-2}^{(0)(1)} - \frac{1}{30} \nabla p_{-4}^{(0)(1)} \right) + \mathbf{r} \left( \frac{4}{15} p_{-4}^{(0)(1)} + \frac{1}{2} p_{-3}^{(0)(1)} + 2p_{-2}^{(0)(1)} \right), \end{aligned} \quad (\text{C1})$$

$$p_1^{(0)} = p_{-2}^{(0)(1)} + p_{-3}^{(0)(1)} + p_{-4}^{(0)(1)}, \quad (\text{C2})$$

$$\begin{aligned} \mathbf{u}_2^{(0)} &= \nabla \times (\mathbf{r}\chi_{-3}^{(0)(2)} + \mathbf{r}\chi_1^{(0)(2)} + \mathbf{r}\chi_2^{(0)(2)}) \\ &\quad + \nabla(\phi_{-4}^{(0)(2)} + \phi_{-3}^{(0)(2)} + \phi_{-2}^{(0)(2)} + \phi_1^{(0)(2)} + \phi_2^{(0)(2)} + \phi_3^{(0)(2)}) \\ &\quad + \frac{r^2}{\lambda_2} \left( \frac{1}{2} \nabla p_{-2}^{(0)(2)} - \frac{1}{30} \nabla p_{-4}^{(0)(2)} + \frac{1}{5} \nabla p_1^{(0)(2)} + \frac{5}{42} \nabla p_2^{(0)(2)} + \frac{1}{12} \nabla p_3^{(0)(2)} \right) \\ &\quad - \frac{\mathbf{r}}{\lambda_2} \left( \frac{4}{15} p_{-4}^{(0)(2)} + \frac{1}{2} p_{-3}^{(0)(2)} + 2p_{-2}^{(0)(2)} + \frac{1}{10} p_1^{(0)(2)} + \frac{2}{21} p_2^{(0)(2)} + \frac{1}{12} p_3^{(0)(2)} \right), \end{aligned} \quad (\text{C3})$$

$$p_2^{(0)} = p_1^{(0)(2)} + p_2^{(0)(2)} + p_3^{(0)(2)} + p_{-2}^{(0)(2)} + p_{-3}^{(0)(2)} + p_{-4}^{(0)(2)}, \quad (\text{C4})$$

$$\begin{aligned} \mathbf{u}_3^{(0)} &= \nabla \times (\mathbf{r}\chi_1^{(0)(3)} + \mathbf{r}\chi_2^{(0)(3)}) + \nabla(\phi_1^{(0)(3)} + \phi_2^{(0)(3)} + \phi_3^{(0)(3)}) \\ &\quad + \frac{r^2}{\lambda_3} \left( \frac{1}{5} \nabla p_1^{(0)(3)} + \frac{5}{42} \nabla p_2^{(0)(3)} + \frac{1}{12} \nabla p_3^{(0)(3)} \right) \\ &\quad - \frac{\mathbf{r}}{\lambda_3} \left( \frac{1}{10} p_1^{(0)(3)} + \frac{2}{21} p_2^{(0)(3)} + \frac{1}{12} p_3^{(0)(3)} \right), \end{aligned} \quad (\text{C5})$$

$$p_3^{(0)} = p_1^{(0)(3)} + p_2^{(0)(3)} + p_3^{(0)(3)}. \quad (\text{C6})$$

**APPENDIX D: EXPRESSIONS FOR THE  $O(\text{Re}_E)$  ELECTRIC POTENTIAL FOR THE SHELL AND CORE DROPS**

$$\begin{aligned}
 \psi_1^{(\text{Re}_E)} &= r^{-1} a_{-1,0}^{(\text{Re}_E)} + r^{-2} (a_{-2,0}^{(\text{Re}_E)} P_{1,0} + a_{-2,1}^{(\text{Re}_E)} P_{1,1} \cos \phi) \\
 &+ r^{-3} (a_{-3,0}^{(\text{Re}_E)} P_{2,0} + a_{-3,1}^{(\text{Re}_E)} P_{2,1} \cos \phi + a_{-3,2}^{(\text{Re}_E)} P_{2,2} \cos 2\phi) \\
 &+ r^{-4} (a_{-4,0}^{(\text{Re}_E)} P_{3,0} + a_{-4,1}^{(\text{Re}_E)} P_{3,1} \cos \phi + a_{-4,2}^{(\text{Re}_E)} P_{3,2} \cos 2\phi + a_{-4,3}^{(\text{Re}_E)} P_{3,3} \cos 3\phi) \\
 &+ r^{-5} (a_{-5,0}^{(\text{Re}_E)} P_{4,0} + a_{-5,1}^{(\text{Re}_E)} P_{4,1} \cos \phi + a_{-5,2}^{(\text{Re}_E)} P_{4,2} \cos 2\phi + a_{-5,3}^{(\text{Re}_E)} P_{4,3} \cos 3\phi), \quad (\text{D1})
 \end{aligned}$$

$$\begin{aligned}
 \psi_2^{(\text{Re}_E)} &= r^{-1} b_{-1,0}^{(\text{Re}_E)} + r^{-2} (b_{-2,0}^{(\text{Re}_E)} P_{1,0} + b_{-2,1}^{(\text{Re}_E)} P_{1,1} \cos \phi) \\
 &+ r^{-3} (b_{-3,0}^{(\text{Re}_E)} P_{2,0} + b_{-3,1}^{(\text{Re}_E)} P_{2,1} \cos \phi + b_{-3,2}^{(\text{Re}_E)} P_{2,2} \cos 2\phi) \\
 &+ r^{-4} (b_{-4,0}^{(\text{Re}_E)} P_{3,0} + b_{-4,1}^{(\text{Re}_E)} P_{3,1} \cos \phi + b_{-4,2}^{(\text{Re}_E)} P_{3,2} \cos 2\phi + b_{-4,3}^{(\text{Re}_E)} P_{3,3} \cos 3\phi) \\
 &+ r^{-5} (b_{-5,0}^{(\text{Re}_E)} P_{4,0} + b_{-5,1}^{(\text{Re}_E)} P_{4,1} \cos \phi + b_{-5,2}^{(\text{Re}_E)} P_{4,2} \cos 2\phi + b_{-5,3}^{(\text{Re}_E)} P_{4,3} \cos 3\phi) \\
 &+ b_{0,0} + r (b_{1,0}^{(\text{Re}_E)} P_{1,0} + b_{1,1}^{(\text{Re}_E)} P_{1,1} \cos \phi) \\
 &+ r^2 (b_{2,0}^{(\text{Re}_E)} P_{2,1} + b_{2,1}^{(\text{Re}_E)} P_{2,1} \cos \phi + b_{2,2}^{(\text{Re}_E)} P_{2,2} \cos 2\phi) \\
 &+ r^3 (b_{3,0}^{(\text{Re}_E)} P_{3,1} + b_{3,1}^{(\text{Re}_E)} P_{3,1} \cos \phi + b_{3,2}^{(\text{Re}_E)} P_{3,2} \cos 2\phi + b_{3,3}^{(\text{Re}_E)} P_{3,3} \cos 3\phi) \\
 &+ r^4 (b_{4,0}^{(\text{Re}_E)} P_{4,1} + b_{4,1}^{(\text{Re}_E)} P_{4,1} \cos \phi + b_{4,2}^{(\text{Re}_E)} P_{4,2} \cos 2\phi + b_{4,3}^{(\text{Re}_E)} P_{4,3} \cos 3\phi), \quad (\text{D2})
 \end{aligned}$$

$$\begin{aligned}
 \psi_3^{(\text{Re}_E)} &= c_{0,0}^{(\text{Re}_E)} + r (c_{1,0}^{(\text{Re}_E)} P_{1,0} + c_{1,1}^{(\text{Re}_E)} P_{1,1} \cos \phi) \\
 &+ r^2 (c_{2,0}^{(\text{Re}_E)} P_{2,1} + c_{2,1}^{(\text{Re}_E)} P_{2,1} \cos \phi + c_{2,2}^{(\text{Re}_E)} P_{2,2} \cos 2\phi) \\
 &+ r^3 (c_{3,0}^{(\text{Re}_E)} P_{3,1} + c_{3,1}^{(\text{Re}_E)} P_{3,1} \cos \phi + c_{3,2}^{(\text{Re}_E)} P_{3,2} \cos 2\phi + c_{3,3}^{(\text{Re}_E)} P_{3,3} \cos 3\phi) \\
 &+ r^4 (c_{4,0}^{(\text{Re}_E)} P_{4,1} + c_{4,1}^{(\text{Re}_E)} P_{4,1} \cos \phi + c_{4,2}^{(\text{Re}_E)} P_{4,2} \cos 2\phi + c_{4,3}^{(\text{Re}_E)} P_{4,3} \cos 3\phi). \quad (\text{D3})
 \end{aligned}$$

**APPENDIX E: ELECTROHYDRODYNAMIC FLOW OF A CONCENTRIC COMPOUND DROP UNDER IMPOSED BACKGROUND UNIFORM FLOW**

Instead of a background Poiseuille flow, if we consider the background flow to be uniform  $V_\infty = V_c e_z$ , then  $k_0 = 1$ ,  $k_1 = 0$ , and  $k_2 = 0$ . Substituting the same, the drop velocity at the leading order is obtained as

$$U_{2,x}^{(0)} = U_{2,y}^{(0)} = 0, \quad U_{2,z}^{(0)} = 1, \quad (\text{E1})$$

$$U_{3,x}^{(0)} = U_{3,y}^{(0)} = 0, \quad U_{3,z}^{(0)} = 1. \quad (\text{E2})$$

Following the procedure outlined in Sec. II D 6, solving for the velocity field at  $O(\text{Re}_E)$  using the above leading-order solution, we obtain

$$U_{2,x}^{(\text{Re}_E)} = U_{2,y}^{(\text{Re}_E)} = U_{2,z}^{(\text{Re}_E)} = 0, \quad (\text{E3})$$

$$U_{3,x}^{(\text{Re}_E)} = U_{3,y}^{(\text{Re}_E)} = U_{3,z}^{(\text{Re}_E)} = 0. \quad (\text{E4})$$

**APPENDIX F: EXPRESSION FOR THE  $O(\text{Ca})$  ELECTRIC POTENTIAL  
IN THE SHELL AND CORE DROPS**

$$\begin{aligned}
 \psi_1^{(\text{Ca})} = & r^{-2}(a_{-2,0}^{(\text{Ca})}P_{1,0} + a_{-2,1}^{(\text{Ca})}P_{1,1} \cos \phi) \\
 & + r^{-3}(a_{-3,0}^{(\text{Ca})}P_{2,0} + a_{-3,1}^{(\text{Ca})}P_{2,1} \cos \phi + a_{-3,2}^{(\text{Ca})}P_{2,2} \cos 2\phi) \\
 & + r^{-4}(a_{-4,0}^{(\text{Ca})}P_{3,0} + a_{-4,1}^{(\text{Ca})}P_{3,1} \cos \phi + a_{-4,2}^{(\text{Ca})}P_{3,2} \cos 2\phi + a_{-4,3}^{(\text{Ca})}P_{3,3} \cos 3\phi) \\
 & + r^{-5}(a_{-5,0}^{(\text{Ca})}P_{4,0} + a_{-5,1}^{(\text{Ca})}P_{4,1} \cos \phi + a_{-5,2}^{(\text{Ca})}P_{4,2} \cos 2\phi + a_{-5,3}^{(\text{Ca})}P_{4,3} \cos 3\phi), \quad (\text{F1})
 \end{aligned}$$

$$\begin{aligned}
 \psi_2^{(\text{Ca})} = & r^{-2}(b_{-2,0}^{(\text{Ca})}P_{1,0} + b_{-2,1}^{(\text{Ca})}P_{1,1} \cos \phi) \\
 & + r^{-3}(b_{-3,0}^{(\text{Ca})}P_{2,0} + b_{-3,1}^{(\text{Ca})}P_{2,1} \cos \phi + b_{-3,2}^{(\text{Ca})}P_{2,2} \cos 2\phi) \\
 & + r^{-4}(b_{-4,0}^{(\text{Ca})}P_{3,0} + b_{-4,1}^{(\text{Ca})}P_{3,1} \cos \phi + b_{-4,2}^{(\text{Ca})}P_{3,2} \cos 2\phi + b_{-4,3}^{(\text{Ca})}P_{3,3} \cos 3\phi) \\
 & + r^{-5}(b_{-5,0}^{(\text{Ca})}P_{4,0} + b_{-5,1}^{(\text{Ca})}P_{4,1} \cos \phi + b_{-5,2}^{(\text{Ca})}P_{4,2} \cos 2\phi + b_{-5,3}^{(\text{Ca})}P_{4,3} \cos 3\phi) \\
 & + r(b_{1,0}^{(\text{Ca})}P_{1,0} + b_{1,1}^{(\text{Ca})}P_{1,1} \cos \phi) \\
 & + r^2(b_{2,0}^{(\text{Ca})}P_{2,0} + b_{2,1}^{(\text{Ca})}P_{2,1} \cos \phi + b_{2,2}^{(\text{Ca})}P_{2,2} \cos 2\phi) \\
 & + r^3(b_{3,0}^{(\text{Ca})}P_{3,1} + b_{3,1}^{(\text{Ca})}P_{3,1} \cos \phi + b_{3,2}^{(\text{Ca})}P_{3,2} \cos 2\phi + b_{3,3}^{(\text{Ca})}P_{3,3} \cos 3\phi) \\
 & + r^4(b_{4,0}^{(\text{Ca})}P_{4,1} + b_{4,1}^{(\text{Ca})}P_{4,1} \cos \phi + b_{4,2}^{(\text{Ca})}P_{4,2} \cos 2\phi + b_{4,3}^{(\text{Ca})}P_{4,3} \cos 3\phi), \quad (\text{F2})
 \end{aligned}$$

$$\begin{aligned}
 \psi_3^{(\text{Ca})} = & r(c_{1,0}^{(\text{Ca})}P_{1,0} + c_{1,1}^{(\text{Ca})}P_{1,1} \cos \phi) \\
 & + r^2(c_{2,0}^{(\text{Ca})}P_{2,0} + c_{2,1}^{(\text{Ca})}P_{2,1} \cos \phi + c_{2,2}^{(\text{Ca})}P_{2,2} \cos 2\phi) \\
 & + r^3(c_{3,0}^{(\text{Ca})}P_{3,0} + c_{3,1}^{(\text{Ca})}P_{3,1} \cos \phi + c_{3,2}^{(\text{Ca})}P_{3,2} \cos 2\phi + c_{3,3}^{(\text{Ca})}P_{3,3} \cos 3\phi) \\
 & + r^4(c_{4,0}^{(\text{Ca})}P_{4,0} + c_{4,1}^{(\text{Ca})}P_{4,1} \cos \phi + c_{4,2}^{(\text{Ca})}P_{4,2} \cos 2\phi + c_{4,3}^{(\text{Ca})}P_{4,3} \cos 3\phi). \quad (\text{F3})
 \end{aligned}$$

**APPENDIX G: VALIDATION OF THE MODEL**

In this section, we validate our analytical solution with the results of Taylor [1] for a neutrally buoyant leaky dielectric single drop in the presence of a uniform electric field and without an imposed background Poiseuille flow. For this, we substitute  $\mathbf{E}_\infty = \mathbf{e}_z$  and  $k_0 = k_1 = k_2 = 0$  in the expressions for  $L_{n,m}^{(\text{Ca})ij}$ , which leads to the following expression for the deformed radius in the single drop limit ( $K \rightarrow 0$ ):

$$r_\Pi = 1 + \text{Ca}M \left\{ \frac{3}{4} \frac{1}{(R_{12} + 2)^2} \left[ R_{12}^2 + 1 - 2S_{12} + \frac{3}{5} \frac{(R_{12} - S_{12})(3\lambda_{12} + 2)}{(\lambda_{12} + 1)} \right] P_{2,0} \right\}. \quad (\text{G1})$$

Next, we consider the case of a single drop migrating and deforming under the action of a background plane Poiseuille flow and without an externally imposed electric field. For this, we substitute  $E_x = E_y = 0$  in Eq. (69) in the expression of the compound drop velocity to get the following expression for a droplet velocity in the single drop limit ( $K \rightarrow 0$ ):

$$\begin{aligned}
 \mathbf{U}_{12} = & \left[ k_0 + \left( \frac{\lambda_{12}}{3\lambda_{12} + 2} \right) k_1 \right] \mathbf{e}_z \\
 & + \text{Ca} \left[ \left( -\frac{k_1 k_2}{210} \right) \frac{(198\lambda_{12}^5 - 1242\lambda_{12}^4 - 7327\lambda_{12}^3 - 6292\lambda_{12}^2 + 1843\lambda_{12} + 2320)}{(3\lambda_{12} + 2)^2(4 + \lambda_{12})(\lambda_{12} + 1)^2} \right] \mathbf{e}_x. \quad (\text{G2})
 \end{aligned}$$

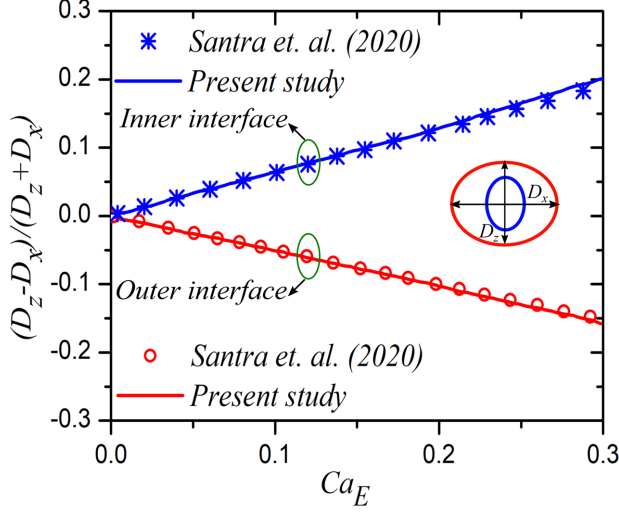


FIG. 20. Variation of  $(D_z - D_x)/(D_z + D_x)$  using the concentric compound drop theory with  $Ca_E$  for the outer and inner interface and comparison of the same with the analytical results of Santra *et al.* [43] for  $R_{12} = 0.033$ ,  $R_{13} = 1$ ,  $S_{12} = 0.44$ ,  $S_{13} = 1$ ,  $\lambda_{12} = 1$ ,  $\lambda_{13} = 1$ , and  $\theta_i = 0$ .

Similarly, substituting the expressions for  $L_{n,m}^{(Ca)(ij)}$  leads to the following expression for the deformed radius in the single drop limit ( $K \rightarrow 0$ ) for a drop deforming under the action of a plane Poiseuille flow and without an externally imposed electric field:

$$r_{\Pi} = 1 + Ca \left\{ \frac{1}{24} \left( \frac{19\lambda_{12} + 16}{\lambda_{12} + 1} \right) k_1 \right\} \cos\phi P_{2,1} - \left\{ \frac{1}{40} \left( \frac{11\lambda_{12} + 10}{\lambda_{12} + 1} \right) k_2 \right\} P_{3,0} + \left\{ \frac{1}{240} \left( \frac{11\lambda_{12} + 10}{\lambda_{12} + 1} \right) k_2 \right\} \cos(2\phi) P_{3,2}. \quad (G3)$$

Equations (G2) and (G3) are in agreement with the previously obtained solution by Chan and Leal [48].

Additionally, we also consider the analytical work of Santra *et al.* [43] for a neutrally buoyant compound drop in an unbounded suspending medium subjected to a uniform electric field. Using our solution for deformed interface shape, we determine the variation of  $(D_z - D_x)/(D_z + D_x)$  with  $Ca_E$ , where  $D_z$  is the length of the shell or core drop along the  $z$  direction and  $D_x$  is the length of the shell or core drop along the  $x$  direction. From the results shown in Fig. 20, we find that the variation of  $(D_z - D_x)/(D_z + D_x)$  with  $Ca_E$  matches well with that of Santra *et al.* [43].

#### APPENDIX H: VALIDATION OF CONCENTRIC COMPOUND DROP THEORY

Previously, Mandal *et al.* [44] have shown that a good agreement is observed between the eccentric compound drop solutions and the concentric compound drop solutions for values of eccentricity  $e < 0.1$ . Based on our solution for  $U_{2,z}$  and  $U_{3,z}$ , we plotted the variation of eccentricity with nondimensional time ( $t$ ) for different values of radius ratio in Fig. 21. The property ratios and other associated parameters are provided in the figure caption. From the plot, it is found that for the nondimensional time range of the order of 10, the eccentricity of the compound drop does not exceed the critical limit of 0.1, and hence, our solution is negligibly affected by the eccentricity up to the aforementioned time limit. The variation of eccentricity with time is almost quantitatively and qualitatively similar for  $R_{12} < S_{12}$  and  $R_{12} > S_{12}$ , and therefore, we have presented only for one case. Indeed, it is to be mentioned that when the compound drop is under the action of a background



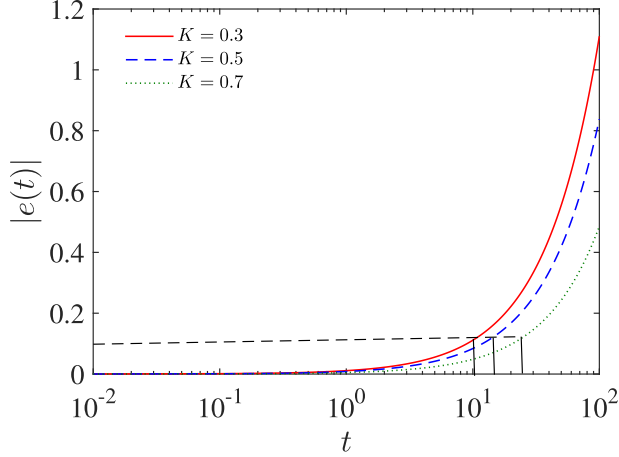


FIG. 21. Variation of eccentricity with nondimensional time for different radius ratio of the concentric compound drop. The rest of the parameters are  $\theta_i = \pi/4$ ,  $R_{12} = 0.01$ ,  $R_{13} = 1$ ,  $S_{12} = 0.63$ ,  $S_{13} = 1$ ,  $\lambda_{12} = 0.35$ ,  $\lambda_{13} = 1$ ,  $x_d = 4$ ,  $H = 10$ ,  $M = 1$ ,  $Ca = 0.1$ , and  $Re_E = 0.1$ .

flow, then the velocities are large enough to be within the valid limit of concentric compound drop theory. In this case, the eccentric compound drop theory [61, 73] should be applied. In Figs. 19 and 21, we show how the aforementioned criterion for the validity of concentric compound drop theory is supported quantitatively by our results.

#### APPENDIX I: ALGEBRAIC EQUATIONS FOR THE ELECTRIC POTENTIAL FIELD USING ECCENTRIC COMPOUND DROP THEORY

The algebraic equations for the unknown coefficients are derived by substituting the expressions for  $\omega_i$  into the boundary conditions Eqs. (78) and (79) and using the orthogonality property of the Gegenbauer polynomials given by [73]

$$\int_{-1}^1 \frac{C_{n+1}^{-\frac{1}{2}}(x)C_{k+1}^{-\frac{1}{2}}(x)}{1-x^2} dx = \frac{2\delta_{nk}}{n(n+1)(2n+1)}. \quad (I1)$$

The linear algebraic equations which are intercoupled in terms of  $(n-1)$ th,  $n$ th, and  $(n+1)$ th mode coefficients are as follows:

$$\begin{aligned} & [-d_{n-1}\mathfrak{R}_{4n} + f_{n-1}\mathfrak{R}_{5n} - g_{n-1}\mathfrak{R}_{6n}](n+1) + d_n\Upsilon_{1n} - f_n\Upsilon_{2n} + g_n\Upsilon_{3n} \\ & + [-d_{n+1}\mathfrak{R}_{7n} + f_{n+1}\mathfrak{R}_{8n} - g_{n+1}\mathfrak{R}_{9n}]n \\ & = 4\sqrt{2}n(n+1)c^2 e^{\mp(n+\frac{1}{2})\xi_1} \sinh \xi_1, \end{aligned} \quad (I2)$$

$$-[f_{n-1} - g_{n-1} + h_{n-1}](n+1) + f_n\Upsilon_{4n} - g_n\Upsilon_{5n} + h_n\Upsilon_{5n} - [f_{n+1} - g_{n+1} + h_{n+1}]n = 0, \quad (I3)$$

$$-d_n\mathfrak{R}_{1n} + [f_n\mathfrak{R}_{2n} + g_n\mathfrak{R}_{3n}]R_{12} = 4\sqrt{2}n(n+1)c^2 e^{\mp(n+\frac{1}{2})\xi_1}, \quad (I4)$$

$$[f_n + g_n]R_{12} - h_nR_{13} = 0, \quad (I5)$$

where

$$\mathfrak{R}_{1n} = \sinh\left(n + \frac{1}{2}\right)\xi_1; \quad \mathfrak{R}_{2n} = e^{(n+\frac{1}{2})(\xi_1-\xi_2)}; \quad \mathfrak{R}_{3n} = e^{-(n+\frac{1}{2})(\xi_1-\xi_2)};$$

$$\mathfrak{R}_{4n} = \cosh\left(n - \frac{1}{2}\right)\xi_1; \quad \mathfrak{R}_{5n} = e^{(n-\frac{1}{2})(\xi_1-\xi_2)}; \quad \mathfrak{R}_{6n} = e^{-(n-\frac{1}{2})(\xi_1-\xi_2)};$$

$$\mathfrak{R}_{7n} = \cosh\left(n + \frac{3}{2}\right)\xi_1; \quad \mathfrak{R}_{8n} = e^{(n+\frac{3}{2})(\xi_1-\xi_2)}; \quad \mathfrak{R}_{9n} = e^{-(n+\frac{3}{2})(\xi_1-\xi_2)};$$

$$\Upsilon_{1n} = (2n + 1) \cosh \xi_1 \cosh\left(n + \frac{1}{2}\right)\xi_1 - \mathfrak{R}_{1n} \sinh \xi_1;$$

$$\Upsilon_{2n} = [(2n + 1) \cosh \xi_1 - \sinh \xi_1] \mathfrak{R}_{2n}; \quad \Upsilon_{3n} = [(2n + 1) \cosh \xi_1 + \sinh \xi_1] \mathfrak{R}_{3n};$$

$$\Upsilon_{4n} = (2n + 1) \cosh \xi_2 - \sinh \xi_2; \quad \Upsilon_{5n} = (2n + 1) \cosh \xi_2 + \sinh \xi_2.$$

#### APPENDIX J: ALGEBRAIC EQUATIONS FOR THE HYDRODYNAMIC FIELD USING ECCENTRIC COMPOUND DROP THEORY

Using Eqs. (82)–(89) together in the boundary conditions Eqs. (90)–(92), we can form the following set of eight algebraic equations for each mode  $n$ :

$$D_n \Lambda_n^1 + E_n \Lambda_n^2 = \Lambda_n^3 \left( \frac{Q_n \Lambda_n^4}{(2n-1)} - \frac{\hat{Q}_n \Lambda_n^5}{(2n+3)} \right) - U_2 \Lambda_n^3 \left( \frac{\Lambda_n^4}{(2n-1)} - \frac{\Lambda_n^5}{(2n+3)} \right), \quad (\text{J1})$$

$$H_n \Lambda_n^1 + I_n \Lambda_n^2 + J_n \Lambda_n^4 + K_n \Lambda_n^5 = 0, \quad (\text{J2})$$

$$(2n-1) \{ (D_n - H_n) \Lambda_n^1 + J_n \Lambda_n^4 \} + (2n+3) \{ (E_n - I_n) \Lambda_n^2 + K_n \Lambda_n^5 \} \\ = -\Lambda_n^3 (Q_n \Lambda_n^4 - \hat{Q}_n \Lambda_n^5) + U_2 \Lambda_n^3 (\Lambda_n^4 - \Lambda_n^5), \quad (\text{J3})$$

$$(2n-1)^2 \{ (D_n - \lambda_2 H_n) \Lambda_n^1 - \lambda_2 J_n \Lambda_n^4 \} + (2n+3)^2 \{ (E_n - \lambda_2 I_n) \Lambda_n^2 - \lambda_2 K_n \Lambda_n^5 \} \\ = \Lambda_n^6 \left( \frac{S_{12}}{R_{12}} - 1 \right) \left[ \frac{(2n+1) \Lambda_n^7}{2} \left\{ c \Omega_{n,k}^1 - c^2 \Omega_{n,k}^2 - \frac{1}{c} \Lambda_k^8 \Omega_{n,k}^3 - \frac{1}{2c} \Lambda_k^9 \Omega_{n,k}^4 \right\} \right. \\ \left. + \Lambda_n^{10} \sinh \xi_1 \left\{ -\frac{c}{2} \Omega_{n,k}^5 + \frac{c^2}{2} \Omega_{n,k}^6 + \frac{1}{2c} \Lambda_k^8 \Omega_{n,k}^7 + \frac{1}{2c} \Lambda_k^9 \Omega_{n,k}^8 \right\} \right] \\ + \Lambda_n^3 \{ (2n-1) Q_n \Lambda_n^4 - (2n+3) \hat{Q}_n \Lambda_n^5 \} - U_2 \Lambda_n^3 \{ (2n-1) \Lambda_n^4 - (2n+3) \Lambda_n^5 \}, \quad (\text{J4})$$

$$H_n \Lambda_n^1 + I_n \Lambda_n^2 + J_n \Lambda_n^4 + K_n \Lambda_n^5 = (U_2 - U_3) \Lambda_n^3 \left( \frac{\Lambda_n^4}{(2n-1)} - \frac{\Lambda_n^5}{(2n+3)} \right), \quad (\text{J5})$$

$$L_n \Lambda_n^4 + M_n \Lambda_n^5 = (U_2 + U_3) \Lambda_n^3 \left( \frac{\Lambda_n^4}{(2n-1)} - \frac{\Lambda_n^5}{(2n+3)} \right), \quad (\text{J6})$$

$$(2n-1) \{ H_n \Lambda_n^1 + (L_n - J_n) \Lambda_n^4 \} + (2n+3) \{ I_n \Lambda_n^2 + (M_n - K_n) \Lambda_n^5 \} = 0, \quad (\text{J7})$$

$$(2n-1)^2 \{ \lambda_2 H_n \Lambda_n^1 + (\lambda_2 J_n - \lambda_3 L_n) \Lambda_n^4 \} + (2n+3)^2 \{ \lambda_2 I_n \Lambda_n^2 + (\lambda_2 K_n - \lambda_3 M_n) \Lambda_n^5 \} \\ = \Lambda_n^6 \left( \frac{S_{12} R_{13}}{R_{12}} - S_{13} \right) \left[ \frac{(2n+1) \Lambda_n^7}{2} \left\{ -\frac{1}{c} \Lambda_k^8 \Omega_{n,k}^3 - \frac{1}{2c} \Lambda_k^9 \Omega_{n,k}^4 \right\} \right. \\ \left. + \Lambda_n^{10} \sinh \xi_2 \left\{ \frac{1}{2c} \Lambda_k^8 \Omega_{n,k}^7 + \frac{1}{2c} \Lambda_k^9 \Omega_{n,k}^8 \right\} \right] \\ + (U_2 - U_3) (\lambda_2 - \lambda_3) \Lambda_n^3 \{ (2n-1) \Lambda_n^4 - (2n+3) \Lambda_n^5 \}. \quad (\text{J8})$$

The notations used in Eqs. (J1)–(J8) have the following expressions:

$$\Lambda_n^1 = e^{(n-\frac{1}{2})\xi}, \quad \Lambda_n^2 = e^{(n+\frac{3}{2})\xi}, \quad \Lambda_n^3 = n(n+1)c^2/\sqrt{2}, \quad \Lambda_n^4 = e^{-(n-\frac{1}{2})\xi},$$

$$\begin{aligned}
 \Lambda_n^5 &= e^{-(n+\frac{3}{2})\xi}, \\
 \Lambda_n^6 &= \frac{n(n+1)(2n+1)}{2\pi}, \quad \Lambda_n^7 = f_n e^{(n+\frac{1}{2})(\xi-\xi_2)} - g_n e^{-(n+\frac{1}{2})(\xi-\xi_2)}, \\
 \Lambda_k^8 &= \sum_{k=0}^N d_k \sinh\left(k + \frac{1}{2}\right) \xi C_k^{\frac{1}{2}}, \quad \Lambda_k^9 = \sum_{k=0}^N d_k \sinh\left(k + \frac{1}{2}\right) \xi C_{k+1}^{-\frac{1}{2}}, \\
 \Lambda_n^{10} &= f_n e^{(n+\frac{1}{2})(\xi-\xi_2)} + g_n e^{-(n+\frac{1}{2})(\xi-\xi_2)}, \\
 Q_n &= 1 + \frac{2c^2}{3R^2}(n-1)(n-2), \quad \hat{Q}_n = 1 + \frac{2c^2}{3R^2}(n+2)(n+3), \\
 \Omega_{n,k}^1(\xi) &= \int_{-1}^1 \frac{x C_{n+1}^{-\frac{1}{2}} C_{k+1}^{-\frac{1}{2}}}{(1-x^2)} dx, \quad \Omega_{n,k}^2(\xi) = \int_{-1}^1 \frac{C_{n+1}^{-\frac{1}{2}} C_{k+1}^{-\frac{1}{2}}}{(\cosh \xi - x)} dx, \\
 \Omega_{n,k}^3(\xi) &= \int_{-1}^1 \frac{(\cosh \xi - x)^{\frac{3}{2}} C_{n+1}^{-\frac{1}{2}} C_{k+1}^{-\frac{1}{2}}}{(1-x^2)^{\frac{3}{2}}} dx, \quad \Omega_{n,k}^4(\xi) = \int_{-1}^1 \frac{(\cosh \xi - x)^{\frac{1}{2}} C_{n+1}^{-\frac{1}{2}} C_{k+1}^{-\frac{1}{2}}}{(1-x^2)} dx, \\
 \Omega_{n,k}^5(\xi) &= \int_{-1}^1 \frac{x C_{n+1}^{-\frac{1}{2}} C_{k+1}^{-\frac{1}{2}}}{(1-x^2)(\cosh \xi - x)} dx, \quad \Omega_{n,k}^6(\xi) = \int_{-1}^1 \frac{C_{n+1}^{-\frac{1}{2}} C_{k+1}^{-\frac{1}{2}}}{(\cosh \xi - x)^2} dx, \\
 \Omega_{n,k}^7(\xi) &= \int_{-1}^1 \frac{(\cosh \xi - x)^{\frac{1}{2}} C_{n+1}^{-\frac{1}{2}} C_{k+1}^{-\frac{1}{2}}}{(1-x^2)^{\frac{3}{2}}} dx, \quad \Omega_{n,k}^8(\xi) = \int_{-1}^1 \frac{C_{n+1}^{-\frac{1}{2}} C_{k+1}^{-\frac{1}{2}}}{(\cosh \xi - x)^{\frac{1}{2}} (1-x^2)} dx.
 \end{aligned}$$

It is important to note that  $\xi = \xi_1$  for Eqs. (J1)–(J4) and  $\xi = \xi_2$  for Eqs. (J5)–(J8). From the above equations, it is clear that the flow field is coupled to the electric potential field by the occurrence of the coefficients  $d_k$ ,  $f_n$ , and  $g_n$ , and hence the summation terms involved are truncated at the same  $N$  as considered earlier.

- 
- [1] G. Taylor, Studies in electrohydrodynamics. I. The circulation produced in a drop by electrical field, *Proc. R. Soc. Lond. A* **291**, 159 (1966).
  - [2] A. Wray, D. T. Papageorgiou, R. V. Craster, K. Sefiane, and O. K. Matar, Electrostatic suppression of the “coffee stain effect,” *Langmuir* **30**, 5849 (2014).
  - [3] D. S. Pillai, K. C. Sahu, and R. Narayanan, Electrowetting of a leaky dielectric droplet under a time-periodic electric field, *Phys. Rev. Fluids* **6**, 073701 (2021).
  - [4] H. A. Stone, A. D. Stroock, and A. Ajdari, Engineering flows in small devices: Microfluidics toward a lab-on-a-chip, *Ann. Rev. Fluid Mech.* **36**, 381 (2004).
  - [5] S. Santra, S. Mandal, and S. Chakraborty, Electrohydrodynamics of confined two-dimensional liquid droplets in uniform electric field, *Phys. Fluids* **30**, 062003 (2018).
  - [6] S. Mandal, S. Chakrabarti, and S. Chakraborty, Effect of nonuniform electric field on the electrohydrodynamic motion of a drop in Poiseuille flow, *Phys. Fluids* **29**, 052006 (2017).
  - [7] P. M. Vlahovska, Electrohydrodynamics of drops and vesicles, *Ann. Rev. Fluid Mech.* **51**, 305 (2019).
  - [8] R. V. Bhalwankar and A. K. Kamra, A wind tunnel investigation of the deformation of water drops in the vertical and horizontal electric fields, *J. Geophys. Res. Atmos* **112**, D10215 (2007).
  - [9] A. Kourmatzis and J. S. Shrimpton, Electrohydrodynamic inter-electrode flow and liquid jet characteristics in charge injection atomizers, *Exp. Fluids* **55**, 1 (2014).
  - [10] S. Torza, R. G. Cox, and S. G. Mason, Electrohydrodynamic deformation and burst of liquid drops, *Phil. Trans. R. Soc. A* **269**, 295 (1971).

- [11] D. A. Saville, Electrohydrodynamics: The Taylor-Melcher leaky dielectric model, *Annu. Rev. Fluid Mech.* **29**, 27 (1997).
- [12] E. Lac and G. M. Homsy, Axisymmetric deformation and stability of a viscous drop in a steady electric field, *J. Fluid Mech.* **590**, 239 (2007).
- [13] R. M. Thaokar, Dielectrophoresis and deformation of a liquid drop in a nonuniform, axisymmetric AC electric field, *Eur. Phys. J. E* **35**, 1 (2012).
- [14] S. D. Deshmukh and R. M. Thaokar, Deformation and breakup of a leaky dielectric drop in a quadrupole electric field, *J. Fluid Mech.* **731**, 713 (2013).
- [15] S. Mandal, K. Chaudhury, and S. Chakraborty, Transient dynamics of confined liquid drops in a uniform electric field, *Phys. Rev. E* **89**, 053020 (2014).
- [16] A. Esmaeeli and M. A. Halim, Electrohydrodynamics of a liquid drop in AC electric fields, *Acta Mech.* **229**, 3943 (2018).
- [17] K. C. Sahu, M. K. Tripathi, J. Chaudhari, and S. Chakraborty, Simulations of a weakly conducting droplet under the influence of an alternating electric field, *Electrophor.* **41**, 1953 (2020).
- [18] G. Supeene, C. R. Koch, and S. Bhattacharjee, Deformation of a droplet in an electric field: Nonlinear transient response in perfect and leaky dielectric media, *J. Colloid Interf. Sci.* **318**, 463 (2008).
- [19] G. Tomar, G. Daniel, G. Biswas, A. Norbert, A. Sharma, F. Durst, S. W. J. W. Welch, and A. Delgado, Two-phase electrohydrodynamic simulations using a volume-of-fluid approach, *J. Comput. Phys.* **227**, 1267 (2007).
- [20] J. A. Lanauze, L. M. Walker, and A. S. Khair, The influence of inertia and charge relaxation on electrohydrodynamic drop deformation, *Phys. Fluids* **25**, 112101 (2013).
- [21] B. Nath, G. Biswas, A. Dalal, and K. C. Sahu, Cross-stream migration of drops suspended in Poiseuille flow in the presence of an electric field, *Phys. Rev. E* **97**, 063106 (2018).
- [22] A. Bandopadhyay, S. Mandal, N. K. Kishore, and S. Chakraborty, Uniform electric-field-induced lateral migration of a sedimenting drop, *J. Fluid Mech.* **792**, 553 (2016).
- [23] E. Yariv and Y. Almog, The effect of surface-charge convection on the settling velocity of spherical drops in a uniform electric field, *J. Fluid Mech.* **797**, 536 (2016).
- [24] D. Palaniappan and P. Daripa, Compound droplet in extensional and paraboloidal flows, *Phys. Fluids* **12**, 2377 (2000).
- [25] H. A. Stone and L. G. Leal, Breakup of concentric double emulsion droplets in linear flows, *J. Fluid Mech.* **211**, 123 (1990).
- [26] J. Draxler and R. Marr, Emulsion liquid membranes part I: Phenomenon and industrial application, *Chem. Eng. Process.* **20**, 319 (1986).
- [27] M. L. Fabiilli, J. A. Lee, O. D. Kripfgans, P. L. Carson, and J. B. Fowlkes, Delivery of water-soluble drugs using acoustically triggered perfluorocarbon double emulsions, *Pharm. Res.* **27**, 2753 (2010).
- [28] J. G. Aston, Gas-filled hollow drops in aerosols, *J. Colloid Interf. Sci.* **38**, 547 (1972).
- [29] M. Balla, M. K. Tripathi, and K. C. Sahu, A numerical study of a hollow water droplet falling in air, *Theor. Comput. Fluid Dyn.* **34**, 133 (2020).
- [30] E. Rushton and G. A. Davies, Settling of encapsulated droplets at low Reynolds numbers, *Int. J. Multiphase Flow* **9**, 337 (1983).
- [31] S. S. Sadhal and H. N. Oguz, Stokes flow past compound multiphase drops: The case of completely engulfed drops/bubbles, *J. Fluid Mech.* **160**, 511 (1985).
- [32] H. Liu, Y. Lu, S. Li, Y. Yu, and K. C. Sahu, Deformation and breakup of a compound droplet in three-dimensional oscillatory shear flow, *Int. J. Multiphase Flow* **134**, 103472 (2021).
- [33] H. N. Gouz and S. S. Sadhal, Fluid dynamics and stability analysis of a compound droplet in an electric field, *Q. J. Mech. Appl. Math.* **42**, 65 (1989).
- [34] T. Tsukada, J. Mayama, M. Sato, and M. Hozawa, Theoretical and experimental studies on the behavior of a compound drop under a uniform DC electric field, *J. Chem. Eng. Jpn.* **30**, 215 (1997).
- [35] A. Behjatian and A. Esmaeeli, Electrohydrodynamics of a liquid column under a transverse electric field in confined domains, *Int. J. Multiphase Flow* **48**, 71 (2013).
- [36] P. Soni, V. A. Juvekar, and V. M. Naik, Investigation on dynamics of double emulsion droplet in a uniform electric field, *J. Electrostat.* **71**, 471 (2013).

- [37] P. Soni, D. Dixit, and V. A. Juvekar, Effect of conducting core on the dynamics of a compound drop in an AC electric field, *Phys. Fluids* **29**, 112108 (2017).
- [38] P. Soni, R. M. Thakkar, and V. A. Juvekar, Electrohydrodynamics of a concentric compound drop in an AC electric field, *Phys. Fluids* **30**, 032102 (2018).
- [39] M. P. Borthakur, G. Biswas, and D. Bandyopadhyay, Dynamics of deformation and pinch-off of a migrating compound droplet in a tube, *Phys. Rev. E* **97**, 043112 (2018).
- [40] M. P. Borthakur, B. Nath, and G. Biswas, Dynamics of a compound droplet under the combined influence of electric field and shear flow, *Phys. Rev. Fluids* **6**, 023603 (2021).
- [41] S. Santra, S. Das, and S. Chakraborty, Electric field-induced pinch-off of a compound droplet in Poiseuille flow, *Phys. Fluids* **31**, 062004 (2019).
- [42] S. Santra, A. Jana, and S. Chakraborty, Electric field modulated deformation dynamics of a compound drop in the presence of confined shear flow, *Phys. Fluids* **32**, 122006 (2020).
- [43] S. Santra, S. Das, and S. Chakraborty, Electrically modulated dynamics of a compound droplet in a confined microfluidic environment, *J. Fluid Mech.* **882**, A23 (2020).
- [44] S. Mandal, A. Bandyopadhyay, and S. Chakraborty, The effect of uniform electric field on the cross-stream migration of a drop in plane Poiseuille flow, *J. Fluid Mech.* **809**, 726 (2016).
- [45] X. Xu and G. M. Homsy, The settling velocity and shape distortion of drops in a uniform electric field, *J. Fluid Mech.* **564**, 395 (2006).
- [46] J. Happel and H. Brenner, *Low Reynolds Number Hydrodynamics: With Special Applications to Particulate Media* (Springer Science & Business Media, Netherlands, 2012).
- [47] L. G. Leal, *Advanced Transport Phenomena: Fluid Mechanics and Convective Transport Processes*, Vol. 7 (Cambridge University Press, Cambridge, UK, 2007).
- [48] P. C. H. Chan and L. G. Leal, The motion of a deformable drop in a second-order fluid, *J. Fluid Mech.* **92**, 131 (1979).
- [49] O. O. Ajayi, A note on Taylor's electrohydrodynamic theory, *Proc. R. Soc. London A* **364**, 499 (1978).
- [50] P. R. Wohl and S. I. Rubinow, The transverse force on a drop in an unbounded parabolic flow, *J. Fluid Mech.* **62**, 185 (1974).
- [51] H. Lamb, *Hydrodynamics* (Cambridge University Press, Cambridge, 1993).
- [52] H. Brenner, The stokes resistance of a slightly deformed sphere, *Chem. Eng. Sci.* **19**, 519 (1964).
- [53] G. Hetsroni and S. Haber, The flow in and around a droplet or bubble submerged in an unbound arbitrary velocity field, *Rheol. Acta* **9**, 488 (1970).
- [54] S. Kim and S. J. Karrila, *Microhydrodynamics: Principles and Selected Applications* (Courier Corporation, North Chelmsford, MA, 2013).
- [55] H. Brenner, The slow motion of a sphere through a viscous fluid towards a plane surface, *Chem. Eng. Sci.* **16**, 242 (1961).
- [56] S. S. Sadhal, A note on the thermocapillary migration of a bubble normal to a plane surface, *J. Colloid Interf. Sci.* **95**, 283 (1983).
- [57] J. Happel and H. Brenner, *Low Reynolds Number Hydrodynamics: With Special Applications to Particulate Media*, Vol. 1 (Springer Science & Business Media, Netherlands, 2012).
- [58] M. Stimson and G. B. Jeffery, The motion of two spheres in a viscous fluid, *Proc. Roy. Soc. London. Ser. A* **111**, 110 (1926).
- [59] E. Wacholder and D. Weihs, Slow motion of a fluid sphere in the vicinity of another sphere or a plane boundary, *Chem. Eng. Sci.* **27**, 1817 (1972).
- [60] D. S. Morton, R. S. Subramanian, and R. Balasubramaniam, The migration of a compound drop due to thermocapillarity, *Phys. Fluid A* **2**, 2119 (1990).
- [61] S. N. Jadhav and U. Ghosh, Thermocapillary effects on eccentric compound drops in Poiseuille flows, *Phys. Rev. Fluids* **6**, 073602 (2021).
- [62] S. Mortazavi and G. Tryggvason, A numerical study of the motion of drops in Poiseuille flow. Part 1. Lateral migration of one drop, *J. Fluid Mech.* **411**, 325 (2000).
- [63] A. Ramachandran and L. Gary Leal, The effect of interfacial slip on the rheology of a dilute emulsion of drops for small capillary numbers, *J. Rheol.* **56**, 1555 (2012).

- [64] O. S. Pak, J. Feng, and H. A. Stone, Viscous marangoni migration of a drop in a Poiseuille flow at low surface Péclet numbers, *J. Fluid Mech.* **753**, 535 (2014).
- [65] M.-F. Ficheux, L. Bonakdar, F. Leal-Calderon, and J. Bibette, Some stability criteria for double emulsions, *Langmuir* **14**, 2702 (1998).
- [66] A. S. Utada, E. Lorenceau, D. R. Link, P. D. Kaplan, H. A. Stone, and D. Weitz, Monodisperse double emulsions generated from a microcapillary device, *Sci.* **308**, 537 (2005).
- [67] R. Pal, Rheology of double emulsions, *J. Colloid Interf. Sci.* **307**, 509 (2007).
- [68] S.-H. Kim, J. W. Kim, J.-C. Cho, and D. A. Weitz, Double-emulsion drops with ultra-thin shells for capsule templates, *Lab Chip* **11**, 3162 (2011).
- [69] Z.-M. Bei, T. Jones, A. Tucker-Schwartz, and D. Harding, Electric field mediated droplet centering, *Appl. Phys. Lett.* **93**, 184101 (2008).
- [70] Z.-M. Bei, T. Jones, and A. Tucker-Schwartz, Forming concentric double-emulsion droplets using electric fields, *J. Electrostat.* **67**, 173 (2009).
- [71] Z. Bei, T. B. Jones, and D. R. Harding, Electric field centering of double-emulsion droplets suspended in a density gradient, *Soft Matter* **6**, 2312 (2010).
- [72] A. K. Tucker-Schwartz, Z. Bei, R. L. Garrell, and T. B. Jones, Polymerization of electric field-centered double emulsion droplets to create polyacrylate shells, *Langmuir* **26**, 18606 (2010).
- [73] S. N. Jadhav and U. Ghosh, Effect of surfactant on the settling of a drop towards a wall, *J. Fluid Mech.* **912**, A4 (2021).